

**APPLICATIONS OF THE QUANTUM DRUDE
OSCILLATOR MODEL FOR DISPERSION
INTERACTIONS AND COMPUTATIONAL
VIBRATIONAL SPECTROSCOPY OF CHARGED
WATER CLUSTERS**

by

Tuguldur T. Odbadrakh

B.S. in Chemistry, West Virginia University, 2012

Submitted to the Graduate Faculty of
the Kenneth P. Dietrich School of Arts and Sciences in partial
fulfillment

of the requirements for the degree of

Doctor of Philosophy

University of Pittsburgh

2018

UNIVERSITY OF PITTSBURGH
KENNETH P. DIETRICH SCHOOL OF ARTS AND SCIENCES

This dissertation was presented

by

Tuguldur T. Odbadrakh

It was defended on

April 10th, 2018

and approved by

Kenneth D. Jordan, Ph.D., Richard King Mellon Professor and Distinguished Professor of
Computational Chemistry

Daniel S. Lambrecht, Ph.D., Assistant Professor

Sean Garrett-Roe, Ph.D., Assistant Professor

John A. Keith, Ph.D., Assistant Professor

Dissertation Director: Kenneth D. Jordan, Ph.D., Richard King Mellon Professor and
Distinguished Professor of Computational Chemistry

APPLICATIONS OF THE QUANTUM DRUDE OSCILLATOR MODEL FOR DISPERSION INTERACTIONS AND COMPUTATIONAL VIBRATIONAL SPECTROSCOPY OF CHARGED WATER CLUSTERS

Tuguldur T. Odbadrakh, PhD

University of Pittsburgh, 2018

The harmonic oscillator model is used as the basis for describing dispersion interactions and as the basis for computation of the vibrational frequencies of the hydronium ion at various levels of hydration. First, configuration interaction, Rayleigh-Schrödinger perturbation theory, and the random-phase approximation are applied to two quantum Drude oscillators coupled through the dipole-dipole interaction. It is found that the RPA gives the exact C_6 dispersion coefficient with only the first excited state included while the other methods require infinite excited states. The dispersion-induced dipole moment is derived from the dipole-dipole and dipole-quadrupole interactions between two Drude oscillators by computing the dipole moment expectation value from the second-order wavefunction, and by an integral over the frequency-dependent polarizability and hyperpolarizability of the oscillators. Finally, the correct C_6 coefficient is recovered from the dispersion-induced dipole moment from the electrostatic Hellmann-Feynman theorem. Then secondly, the harmonic oscillator model is used as the basis for computing the vibrational frequencies of cryogenically-cooled, gas-phase $\text{H}^+(\text{H}_2\text{O})_{n=1,4,10,21}$ clusters. The OH stretching frequencies are found to red shift dramatically due to the cubic coupling between the OH stretching modes and due to an inductive interaction from the electric field of the hydration environment. Finally, the role of the electric field in the proton-transfer mechanism in water is discussed.

TABLE OF CONTENTS

1.0 INTRODUCTION	1
1.1 The Drude Oscillator Model	2
1.1.1 The One-Dimensional Quantum Drude Oscillator	3
1.1.2 The Ladder Operator Formalism	4
1.1.3 Computation of the dipole polarizability	6
1.1.4 Long-Range Interactions Between Two Molecules	7
1.2 The Vibrational Problem	12
1.2.1 The Vibrational Hamiltonian For an Arbitrary System	12
1.2.2 Solutions of the Vibrational Problem	14
2.0 APPLICATION OF ELECTRONIC STRUCTURE METHODS TO COUPLED DRUDE OSCILLATORS	17
2.1 Introduction	17
2.2 Methodology	18
2.3 Applications of Electronic Structure Methods to the Drude Oscillator Problem	19
2.3.1 Configuration interaction, Rayleigh-Schrödinger perturbation theory, and CCD	20
2.3.2 The Random-Phase Approximation	22
2.4 Conclusion	24
3.0 DISPERSION DIPOLES FOR COUPLED DRUDE OSCILLATORS .	25
3.1 Introduction	25
3.2 Theory	26
3.3 Conclusions	31

4.0 FIELD-EFFECT ORIGINS OF THE HYDRATION-INDUCED SHIFTS OF THE VIBRATIONAL SPECTRAL SIGNATURES OF THE HYDRONIUM ION IN GAS-PHASE PROTONATED WATER CLUSTERS	33
4.1 Introduction	34
4.2 The Elementary Aqueous Cations	35
4.2.1 The Hydronium Ion and Its OH Stretching Vibrations	36
4.3 Hydration-Induced Shifts in the Hydronium Ion's OH Stretching Frequencies	39
4.3.1 The field effect in the proton-transfer mechanism in water	48
4.4 Extrapolating the Cluster Model to Bulk Water	52
BIBLIOGRAPHY	55

LIST OF TABLES

4.1	Cubic coupling constants involving the three OH stretching vibrations of the hydronium ion (cm^{-1}).	38
4.2	The anharmonicity constants χ_{ij} contributing to the 3-mode model frequencies and VPT2 frequencies.	38
4.3	Harmonic, 3-mode model, and VPT2 vibrational frequencies for the asymmetric OH stretching modes a_1 and a_2 , and the symmetric OH stretching mode s of the bare gas-phase hydronium ion.	39
4.4	The SAPT2 decomposition of the interactions between the hydronium ion and its first hydration shell (n4) and its first two hydration shells (n10c) in units of kcal/mol.	43
4.5	Vibrational frequencies of the hydronium ion's three OH stretching modes in the bare ion (n1), with its first hydration shell (n4), and with its first and second hydration shells (n10c). The symmetric stretch mode is s while the doubly degenerate asymmetric stretch modes are a_1 and a_2	46
4.6	The full VPT2 anharmonicity constants involving the hydronium ion's three OH stretching modes in the bare ion (n1), with its first hydration shell (n4), and with its first and second hydration shells (n10c).	47
4.7	The cubic force constants of the symmetric and doubly-degenerate asymmetric mode of hydronium in the bare ion (1), with its first hydration shell (n4), and with its first and second hydration shells (n10c).	48

LIST OF FIGURES

1.1	The harmonic potential, and the first four eigenvalues (E_{0-3}) and eigenfunctions (ψ_{0-3}) of the quantum Drude oscillator.	4
1.2	Two arbitrary molecules centered at A and B , with the electrons at a and b [1].	8
2.1	Interaction energy of two Drude oscillators coupled through the dipole-dipole interaction calculated with the basis (A) $ 00\rangle, 11\rangle$; (B) $ 00\rangle, 11\rangle, 20\rangle, 02\rangle, 22\rangle$; (C) $ 00\rangle, 11\rangle, 20\rangle, 02\rangle, 22\rangle, 13\rangle, 31\rangle, 33\rangle$, compared to (D) the exact interaction energy.	21
2.2	(A) Fourth-order exclusion principle violating interaction diagram appearing in the RPA. $ 0\rangle$ and $ 1\rangle$ correspond to oscillator 1, while $ 0'\rangle$ and $ 1'\rangle$ correspond to oscillator 2. (B) Shows a fourth-order contribution to the RSPT involving excitation into the $ 22\rangle$ level.	24
3.1	Dispersion-induced change in the charge densities of two interacting one-dimensional Drude oscillators at a distance of $12 a_0$ and with $k = 0.16$ a.u., $q = 0.5$ a.u., and $m = 1$ a.u.	28
3.2	The quadrupolar charge distortion due to dipole-dipole coupling of two one-dimensional Drude oscillators at a separation of $12 a_0$ and with the parameters as used in Figure 3.1.	29
3.3	Dispersion-induced change in the charge densities of two interacting 3D Drude oscillators separated by a distance of $12 a_0$ and with the parameters specified in the text.	31
4.1	The normal modes of an isolated hydronium ion computed at the B3LYP/6-31+G(d) level of theory.	37

4.2	The vibrational spectra of the n1 , n4 , and n21 clusters	40
4.3	Gas-phase geometries used in the potential energy scan of the hydronium ion's OH bond. The structures were fully optimized at the B3LYP/6-31+G(d) level of theory for n1 , n4 , and n21 . For n4c and n10c , the geometries were extracted from the fully relaxed n21 geometry followed by optimization of the hydronium ion's OH bonds while freezing all other degrees of freedom.	41
4.4	The B3LYP/6-31+G(d) potential energy curve of the OH bond of H_3O^+ under the various hydration environments stated in the text.	41
4.5	The interaction energy contributions as a function of the proton displacement.	44
4.6	Interaction-induced electron density changes calculated at the B3LYP/6-31+G(d) level of theory, with the positive change in electron density colored blue and negative change in electron density colored red.	45
4.7	Schematic of the Zundel ion under the influence of proton acceptors.	50
4.8	Solid lines: scans for the potential energy for displacement of the central proton between the special pair of O atoms for H_9O_4^+ ion (blue), $\text{H}_{11}\text{O}_5^+$ (green), and the Zundel-based isomer of $\text{H}_{13}\text{O}_6^+$ (red) evaluated at the MP2/aug-cc-pVDZ level of theory; dotted lines: potentials for proton displacement in the isolated H_5O_2^+ Zundel ion placed in uniform electric fields with magnitudes simulating those of the hydration shell.	51
4.9	A one-dimensional cut through the charge density difference of the Zundel ion under different external electric fields computed at the B3LYP/aug-cc-pVTZ level of theory, overlaid with the central proton's potential energy curve, as well as the three-dimensional density difference isosurface.	52
4.10	The vibrational spectra of $\text{H}^+(\text{H}_2\text{O})_{n=21,24,28}$ clusters compared to the spectra of bulk water and bulk dilute acid.	53

1.0 INTRODUCTION

This document describes my work in two different but related areas of theoretical chemistry; therefore, the document is broken into two broad sections: one on the Drude oscillator model and one on the vibrational spectroscopy of protonated water clusters. These two seemingly unrelated fields at the core are based on the same Hamiltonian (one which is based on the harmonic oscillator model). The Drude oscillator model utilizes the harmonic oscillator model by directly defining a quadratic electron-nucleus interaction, leading to identical eigenfunctions and eigenvalues as the harmonic oscillator model. This model is part of our research group’s efforts to coarse-grain the dispersion interaction between small gas-phase clusters and an excess electron, such as the dipole-bound anion of HCN [2]. Later, the Drude oscillator model was used to describe the bound anions of water clusters, where the inclusion of the dispersion interaction in the model Hamiltonian resulted in binding energies comparable to the CCSD(T) method [3]. When I joined the group, the application of the quantum Drude oscillator model to fully quantum mechanical calculations was in its beginning stages, and therefore no previous work on the application of electronic structure methods to quantum Drude oscillators existed in the literature, except for its application in the many-body polarization and dispersion interactions in diffusion Monte Carlo (DMC) and path-integral molecular dynamics (PIMD) simulations by Jones, et al. [4], as well as its use in correcting density-functional theory to accurately describe dispersion interactions [5, 6]. Due to the simple nature of the Hamiltonian, the Drude oscillator model is a good start for learning the standard electronic structure methods, and it is for this reason that I began my Ph.D. research with the treatment of quantum Drude oscillators.

The computational vibrational spectroscopy method used in Chapter 4 is also based on the harmonic oscillator Hamiltonian. However, it is different from the Drude oscilla-

tor Hamiltonian in that the vibrational Hamiltonian is expressed in terms of normal mode displacements, which are themselves linear combinations of nuclear displacements. My contributions to the study of the vibrational spectra of protonated water clusters is part of a long-standing collaboration between the theory group of Dr. Kenneth Jordan and the experimental group of Dr. Mark Johnson at the Yale University on the vibrational spectroscopy of cryogenically-cooled, gas-phase clusters. Examples of previous publications resulting from this collaboration can be found in References [7, 8, 9, 10]. The remainder of this chapter is structured as follows: Section 1.1.1 describes the one-dimensional Drude oscillator and its wavefunctions and energies. Then the ladder operator formalism is described in Section 1.1.2 and applied to the computation of the static dipole polarizability of the Drude oscillator in Section 1.1.3. Then the theory of long-range intermolecular interactions is reviewed in Section 1.1.4. Section 1.2 sets up the vibrational problem and describes the potential energy function. Finally, the second-order vibrational perturbation-theory is described.

1.1 THE DRUDE OSCILLATOR MODEL

A Drude oscillator consists of a displaceable pseudo-electron coupled harmonically to a pseudo-nucleus through a force constant k [11]. In general the nucleus is fixed and the electron is free to displace around its equilibrium position. The pseudo-electron's classical equilibrium position is at its energy minimum, and an external electric field can shift the position of this minimum, thereby polarizing the Drude pseudo-atom and producing a dipole moment. The dipole-polarizable property of this simple model has recently seen widespread utilization in classical molecular dynamics simulations, including many-body polarization effects in the cell membrane dipole potential [12], DNA base pairs [13], long-timescale simulations of macromolecules and proteins [14], as well as in describing polarizable molecular ionic liquids [15]. In addition to its adoption in classical force-fields the Drude oscillator model has been generalized to treat coarse-grained polarization and dispersion interactions in quantum systems such as the interaction between an excess electron and water clusters [2, 3]. The fully quantum mechanical Drude oscillator models the dispersion interaction

between atoms and molecules and has been successfully used to correct density-functional theory (DFT) for dispersion interactions [16]. It has also been used to describe many-body polarization and dispersion interactions in path integral molecular dynamics (PIMD) and diffusion Monte Carlo (DMC) simulations [17].

This section describes the theoretical foundations of the quantum Drude oscillator model of long-range dispersion interactions. First, the one-dimensional quantum Drude oscillator is described and connected to the harmonic oscillator model in Subsection 1.1.1. Subsection 1.1.2 describes the ladder operator formalism which greatly simplifies the evaluation of integrals in the Drude oscillator model. Lastly, the theoretical formulation of long-range intermolecular interactions is detailed in terms of the multipole expansion of the Coulomb operator along with a perturbation theory interpretation of the various types of intermolecular interactions.

1.1.1 The One-Dimensional Quantum Drude Oscillator

The Hamiltonian describing a one-dimensional Drude oscillator displacing along the z-axis is

$$\hat{H} = \frac{1}{2m}\hat{p}^2 + \frac{1}{2}k\hat{z}^2 \tag{1.1}$$

where \hat{p} is the momentum operator for the displaceable negative charge, \hat{z} is the displacement operator for the displaceable negative charge, m is the effective mass and k is the force constant of the harmonic potential coupling the displaceable negative charge to its positive pseudo-nucleus. The force constant is related to the effective mass m and frequency ω by $k = m\omega^2$. The solution to the time-independent Schrödinger equation

$$E\psi(z) = \hat{H}\psi(z) \tag{1.2}$$

is identical to the solution for the quantum harmonic oscillator, so the wavefunction for the n th state is

$$\psi_n(z) = \frac{1}{\sqrt{2^n n!}} \left(\frac{m\omega}{\pi\hbar}\right)^{\frac{1}{4}} H_n\left(\sqrt{\frac{m\omega}{\hbar}}z\right) e^{-\frac{m\omega}{2\hbar}z^2} \tag{1.3}$$

where n is the quantized energy level and can take any positive integer value including 0. H_n is a Hermite polynomial of order n , \hbar is the reduced Planck constant, and ω is the vibrational frequency of the oscillator. Then the energy levels of the quantum Drude oscillator are

$$E_n = \hbar\omega \left(n + \frac{1}{2} \right), \quad (1.4)$$

resulting in evenly-spaced energy levels ($E_n - E_{n-1} = \hbar\omega$), as well as a zero-point energy (ZPE)

$$E_{\text{ZPE}} = \frac{1}{2}\hbar\omega. \quad (1.5)$$

Figure 1.1 shows the first four wavefunctions and their energies superimposed on the po-

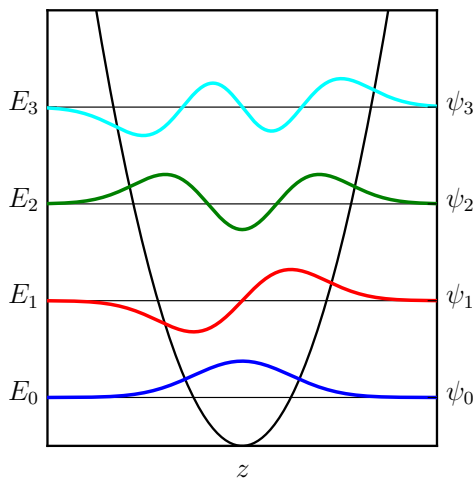


Figure 1.1: The harmonic potential, and the first four eigenvalues (E_{0-3}) and eigenfunctions (ψ_{0-3}) of the quantum Drude oscillator.

tential coupling the pseudo-electron to the pseudo-nucleus.

1.1.2 The Ladder Operator Formalism

The ladder operator formalism is an extremely useful method of treating the harmonic oscillator Schrödinger equation and is akin to the second quantization method of many-body

systems and quantum field theory. The ladder operators are defined using complex linear combinations of the momentum and position operators as

$$\hat{a} = \sqrt{\frac{m\omega}{2\hbar}} \left(\hat{z} + \frac{i}{m\omega} \hat{p} \right) \quad (1.6)$$

$$\hat{a}^\dagger = \sqrt{\frac{m\omega}{2\hbar}} \left(\hat{z} - \frac{i}{m\omega} \hat{p} \right) \quad (1.7)$$

where \hat{a}^\dagger is the "ladder-up" operator and \hat{a} is the "ladder down" operator. The effects of these operators on an eigenstate n of the Hamiltonian in Equation 1.1 are

$$\hat{a} |n\rangle = \sqrt{n} |n-1\rangle \quad (1.8)$$

$$\hat{a}^\dagger |n\rangle = \sqrt{n+1} |n+1\rangle \quad (1.9)$$

where $|n\rangle$ is the wavefunction of state n in "bracket" notation. Then the momentum and position operators can be written as linear combinations of the ladder operators as

$$\hat{p} = i\sqrt{\frac{\hbar}{2m\omega}} (\hat{a}^\dagger - \hat{a}) \quad (1.10)$$

$$\hat{z} = \sqrt{\frac{\hbar}{2m\omega}} (\hat{a}^\dagger + \hat{a}). \quad (1.11)$$

These definition can be used to simplify the evaluation of integrals to that of evaluating overlap integrals of the orthogonal harmonic oscillator wavefunctions. For example, a simple position expectation value can be written as

$$\begin{aligned} \langle z \rangle &= \langle i | \sqrt{\frac{\hbar}{2m\omega}} (\hat{a}^\dagger + \hat{a}) | j \rangle \\ &= \sqrt{\frac{\hbar}{2m\omega}} (\langle i | \hat{a}^\dagger | j \rangle + \langle i | \hat{a} | j \rangle) \\ &= \sqrt{\frac{\hbar}{2m\omega}} (\sqrt{j+1} \langle i | j+1 \rangle + \sqrt{j} \langle i | j-1 \rangle) \\ &= \sqrt{\frac{\hbar}{2m\omega}} (\sqrt{j+1} \delta_{i,j+1} + \sqrt{j} \delta_{i,j-1}) \end{aligned} \quad (1.12)$$

where δ is the Kronecker delta function. We now demonstrate the use of these operators in the calculation of the dipole-polarizability of the quantum Drude oscillator.

1.1.3 Computation of the dipole polarizability

The second-order perturbation theory for the dipole-polarizability of the Drude oscillator is derived from the multipole expansion of the interaction of an oscillator with an applied electric field. The resulting expression is

$$\alpha_{\alpha\beta} = \sum_i \left(\frac{\langle 0|\hat{\mu}_\alpha|i\rangle \langle i|\hat{\mu}\rangle_\beta|0\rangle}{E_i^{(0)} - E_0^{(0)}} + \frac{\langle 0|\hat{\mu}_\beta|i\rangle \langle i|\hat{\mu}_\alpha|0\rangle}{E_i^{(0)} - E_0^{(0)}} \right) \quad (1.13)$$

where the Einstein summation notation was used. The dipole moment operator is defined in three dimensions as $\hat{\mu} = q\hat{\mathbf{r}}$ for the quantum Drude oscillator, where q is the negative charge of the oscillator, and \mathbf{r} is the displacement of the negative charge relative to the positive charge. In one dimension (along the z-axis), the dipole moment operator becomes

$$\hat{\mu}_z = q\hat{z} = q\sqrt{\frac{\hbar}{2m\omega}} (\hat{a}^\dagger + \hat{a}). \quad (1.14)$$

Substituting in this expression into Equation 1.13 in one dimension along the z-axis, and evaluating the overlap integrals resulting from the ladder operators gives

$$\alpha_{zz} = \frac{q^2}{k} = \frac{q^2}{m\omega^2} \quad (1.15)$$

which is the zz component of the dipole polarizability. It is important to note that the dipole moment operator brings in only one displacement operator, so the only nonzero contributions in the sum-over-states are the $|0\rangle \rightarrow |1\rangle$ integrals. Thus for the quantum Drude oscillator, only the first excited state is needed to compute its exact dipole polarizability.

1.1.4 Long-Range Interactions Between Two Molecules

The theory of long-range intermolecular interactions began when van der Waals corrected the ideal gas law $PV = RT$ to include the effects of the incompressible volume of the particles and the attractive interactions between the particles [1]. The volume occupied by the particles themselves, b was subtracted from the volume term, V , to correct the available volume for movement. The long-range interactions between the particles is accounted for by modifying the pressure term, P , to include the decrease in magnitude from the attractive interactions. Thus the "van der Waals equation" was

$$\left(P + \frac{1}{V^2}\right)(V - b) = RT \quad (1.16)$$

and its application as an empirical formula was successful in describing the gas-liquid phase change of molecules. Since then, a variety of different long-range interactions have been classified for atoms and molecules. These include the electrostatic interaction, the induction interaction, and the dispersion interaction. The electrostatic interaction is simply the Coulomb interaction between the static charge densities of the interacting particles. The induction interaction is the response of one particle to the static electric field of the other particle and results in a polarization of the charge density. Finally, but not least, is the dispersion interaction which is described as the stabilizing interaction arising from the correlated fluctuations of the charge densities of the particles. This section describes the important aspects of the theory of intermolecular forces at long range where there is no significant overlap of electron densities.

Consider a system of two arbitrary molecules A and B at positions \mathbf{A} and \mathbf{B} with the electrons at positions $\mathbf{A} + \mathbf{a}$ and $\mathbf{B} + \mathbf{b}$ as shown in Figure 1.2. The electric potential of molecule A measured at \mathbf{B} is given by

$$V^A(\mathbf{B}) = \sum_a \frac{e_a}{4\pi\epsilon_0|\mathbf{B} - \mathbf{A} - \mathbf{a}|} \quad (1.17)$$

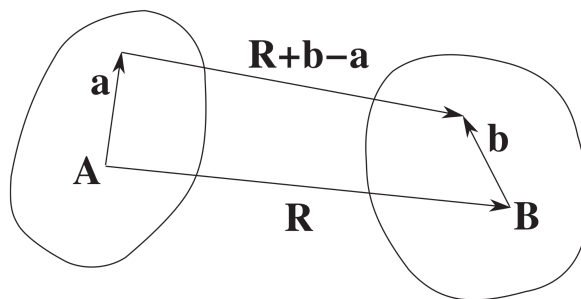


Figure 1.2: Two arbitrary molecules centered at \mathbf{A} and \mathbf{B} , with the electrons at \mathbf{a} and \mathbf{b} [1].

where the sum goes over all electrons a . Defining the separation between the centers of the two molecules as $\mathbf{R} = \mathbf{B} - \mathbf{A}$ and expanding the potential in a Taylor series around \mathbf{A} gives

$$\begin{aligned}
 V^A(\mathbf{B}) &= \sum_a \frac{e_a}{4\pi\epsilon_0} \left\{ \frac{1}{R} - a_\alpha \nabla_\alpha \frac{1}{R} + \frac{1}{2} a_\alpha a_\beta \nabla_\alpha \nabla_\beta \frac{1}{R} - \dots \right\} \\
 &= Tq^A - T_\alpha \hat{\mu}_\alpha^A + \frac{1}{3} T_{\alpha\beta} \hat{\Theta}_{\alpha\beta}^A - \dots + \frac{(-1)^n}{(2n-1)!!} T_{\alpha\beta\dots\nu}^{(n)} \hat{\zeta}_{\alpha\beta\dots\nu}^{A(n)} + \dots
 \end{aligned} \tag{1.18}$$

where the Einstein summation notation was used and the successive derivatives of the potential have been defined as the coupling tensors

$$T = \frac{1}{4\pi\epsilon_0} \frac{1}{R}, \tag{1.19}$$

$$T_\alpha = \frac{1}{4\pi\epsilon_0} \nabla_\alpha \frac{1}{R}, \tag{1.20}$$

$$T_{\alpha\beta} = \frac{1}{4\pi\epsilon_0} \nabla_\alpha \nabla_\beta \frac{1}{R}, \dots \tag{1.21}$$

$$T_{\alpha\beta\dots\nu} = \frac{1}{4\pi\epsilon_0} \nabla_\alpha \nabla_\beta \dots \nabla_\nu \frac{1}{R}. \tag{1.22}$$

Equation 1.18 above is the multipole expansion of the electric potential of molecule A measured at \mathbf{B} . The first term is the electric potential from a point charge q , the second term is the electric potential from a dipole moment $\hat{\mu}_\alpha^A = q^A \mathbf{a}$, and the third term is the electric potential from a quadrupole moment $\hat{\Theta}_{\alpha\beta}^A$, and so on to infinite multipoles. Now the electric potential of molecule A is written as a function of its multipole moments and the separation

between the centers of the two molecules, \mathbf{R} . The operator for the interaction of an arbitrary molecule with an arbitrary non-uniform electric potential V is

$$\hat{H}_{\text{int}} = qV + \hat{\mu}_\alpha V_\alpha + \frac{1}{3}\hat{\Theta}_{\alpha\beta}V_{\alpha\beta} + \dots \quad (1.23)$$

where

$$V_\alpha = \nabla_\alpha V, \quad (1.24)$$

$$V_{\alpha\beta} = \nabla_\alpha \nabla_\beta V, \dots \quad (1.25)$$

Substituting in the multipole expansion of the the electric potential of molecule A gives the interaction energy in terms of the interactions between the multipoles of the two molecules through the coupling tensors, T . For two neutral molecules, dropping the monopole terms involving q and using the appropriate expressions for the electric potential gradients gives

$$\hat{H}_{\text{int}} = -\hat{\mu}_\alpha^A T_{\alpha\beta} \hat{\mu}_\beta^B - \frac{1}{3} \left(\hat{\mu}_\alpha^A T_{\alpha\beta\gamma} \hat{\Theta}_{\beta\gamma}^B - \hat{\Theta}_{\alpha\beta}^A T_{\alpha\beta\gamma} \hat{\mu}_\gamma^B \right) + \dots \quad (1.26)$$

Then it is clear that for a system of two neutral molecules, the interaction energy starts with the stabilizing dipole-dipole interaction through the second derivative of the Coulomb potential ($T_{\alpha\beta}$), followed by the dipole-quadrupole interactions through the third derivatives of the Coulomb potential ($T_{\alpha\beta\gamma}$), and so on to infinite multipole interactions.

It is instructive to discuss the perturbation-theory (PT) solution of the Schrödinger equation for a system of two arbitrary molecules A and B with non-overlapping electron densities. The Hamiltonian derived in Equation 1.26 is partitioned as

$$\hat{H} = \hat{H}_A^{(0)} + \hat{H}_B^{(0)} + \hat{V} \quad (1.27)$$

where $\hat{H}_A^{(0)}$ and $\hat{H}_B^{(0)}$ are the Hamiltonians for the isolated molecules A and B , and \hat{V} is the interaction operator shown in Equation 1.26. The wavefunction is then taken as a product wavefunction $\Psi_{ij}(\mathbf{a}, \mathbf{b}) = \psi_i(\mathbf{a})\psi_j(\mathbf{b})$ of the eigenfunctions of the unperturbed Hamiltonians, as

$$\left(\hat{H}_A^{(0)} + \hat{H}_B^{(0)} \right) |ij\rangle = \left(E_{A_i}^{(0)} + E_{B_j}^{(0)} \right) |ij\rangle \quad (1.28)$$

where i is the quantum number of molecule A and j is the quantum number of molecule B , and the ground state denoted by $|00\rangle$ in the bracket notation. The standard Rayleigh-Schrödinger perturbation theory (RSPT) first- and second-order energy corrections are

$$E^{(1)} = \langle 00 | \hat{V} | 00 \rangle \quad (1.29)$$

$$E^{(2)} = \sum_{i,j \neq 0} \frac{\langle 00 | \hat{V} | ij \rangle \langle ij | \hat{V} | 00 \rangle}{E_{|00\rangle}^{(0)} - E_{|ij\rangle}^{(0)}} \quad (1.30)$$

where $|ij\rangle$ is an excited-state wavefunction in the product basis with molecule A in its i th excited-state and with molecule B in its j th excited-state, and $E_{|ij\rangle}^{(0)}$ is the energy of the unperturbed state $|ij\rangle$. The second-order energy correction requires a sum over all excited states where $j+i \neq 0$, giving two types of integrals in the numerator. Based on the excitations of the two molecules, the second-order energy correction can be decomposed into

$$E_{\text{ind}}^{(2)} = \sum_{i \neq 0} \left(\frac{\langle 00 | \hat{V} | i0 \rangle \langle i0 | \hat{V} | 00 \rangle}{E_{|00\rangle}^{(0)} - E_{|i0\rangle}^{(0)}} + \frac{\langle 00 | \hat{V} | 0i \rangle \langle 0i | \hat{V} | 00 \rangle}{E_{|00\rangle}^{(0)} - E_{|0i\rangle}^{(0)}} \right), \quad (1.31)$$

$$E_{\text{disp}}^{(2)} = \sum_{i,j \neq 0} \frac{\langle 00 | \hat{V} | ij \rangle \langle ij | \hat{V} | 00 \rangle}{E_{|00\rangle}^{(0)} - E_{|ij\rangle}^{(0)}}, \quad (1.32)$$

where $E_{\text{ind}}^{(2)}$ is the induction term and $E_{\text{disp}}^{(2)}$ is the dispersion term. The induction term is named as such because the integrals describing the change in energy require excitations of one molecule while the other stays in its ground state, which can be interpreted as the polarization of one molecule due to the electric field of the other. The dispersion term is defined as such because the integrals involve both molecules in their excited states. The first-order wavefunction correction which gives the second-order energy correction above can also be partitioned as

$$|00\rangle_{\text{ind}}^{(1)} = \sum_{i \neq 0} \left(\frac{\langle 00 | \hat{V} | i0 \rangle}{E_{|00\rangle}^{(0)} - E_{|i0\rangle}^{(0)}} |i0\rangle + \frac{\langle 00 | \hat{V} | 0i \rangle}{E_{|00\rangle}^{(0)} - E_{|0i\rangle}^{(0)}} |0i\rangle \right), \quad (1.33)$$

$$|00\rangle_{\text{disp}}^{(1)} = \sum_{i,j \neq 0} \frac{\langle 00 | \hat{V} | ij \rangle}{E_{|00\rangle}^{(0)} - E_{|ij\rangle}^{(0)}} |ij\rangle. \quad (1.34)$$

Here, it is even more clear that the induction interaction polarizes one molecule through excitations while the dispersion interaction arises from simultaneous excitations of both molecules.

There is an alternate way to compute the dispersion interaction energy for arbitrary dimers from the response properties of the molecules [18] as described below. The approximate second-order dispersion energy in Equation 1.31 can be written with just the dipole-dipole operator as

$$E_{\text{disp}}^{(2)} = - \sum_{i+j \neq 0} \frac{\langle 00 | \hat{\mu}_{\alpha}^A T_{\alpha\beta} \hat{\mu}_{\beta}^B | ij \rangle \langle ij | \hat{\mu}_{\gamma}^A T_{\gamma\delta} \hat{\mu}_{\delta}^B | 00 \rangle}{E_{i0}^A + E_{j0}^B} \quad (1.35)$$

where $E_{i0}^A = E_i^{(0)} - E_0^{(0)}$. The integrals are separable between the two molecules due to the adoption of a product wavefunction, so the above dispersion energy can be written as

$$E_{\text{disp}}^{(2)} = -T_{\alpha\beta} T_{\gamma\delta} \sum_{i+j \neq 0} \frac{\langle 0 | \hat{\mu}_{\alpha}^A | i \rangle \langle i | \hat{\mu}_{\gamma}^A | 0 \rangle \langle 0 | \hat{\mu}_{\beta}^B | j \rangle \langle j | \hat{\mu}_{\delta}^B | 0 \rangle}{E_{i0}^A + E_{j0}^B}. \quad (1.36)$$

Substituting the dipole polarizabilities of A and B and using the integral identity

$$\frac{1}{A+B} = \frac{2}{\pi} \int_0^{\infty} \frac{AB}{(A^2 + \nu^2)(B^2 + \nu^2)} d\nu \quad (1.37)$$

gives the Casimir-Polder expression for the dispersion interaction

$$E_{\text{disp}}^{(2)} = \frac{\hbar}{2\pi} T_{\alpha\beta} T_{\gamma\delta} \int_0^{\infty} \alpha_{\alpha\gamma}^A(i\nu) \alpha_{\beta\delta}^B(i\nu) d\nu. \quad (1.38)$$

We see here that the dispersion energy can be expressed in terms of the frequency-dependent dipole polarizabilities of the interacting Drude oscillators, when coupled through the dipole-dipole coupling tensors $T_{\alpha\beta}$ and $T_{\gamma\delta}$.

1.2 THE VIBRATIONAL PROBLEM

1.2.1 The Vibrational Hamiltonian For an Arbitrary System

The energy and wavefunction of a molecule or a cluster of molecules are obtained through solving the Schrödinger equation

$$\hat{H}\Psi(\mathbf{R}_i, \mathbf{r}_i) = E\Psi(\mathbf{R}_i, \mathbf{r}_i) \quad (1.39)$$

where $\Psi(\mathbf{R}_i, \mathbf{r}_i)$ is the wavefunction of the system as a function of the nuclear degrees of freedom \mathbf{R}_i and the electronic degrees of freedom \mathbf{r}_i for all i atoms, and \hat{H} is the Hamiltonian operator which is defined as

$$\hat{H} = \sum_i \frac{1}{2}P_i^2 + \sum_i \frac{1}{2}p_i^2 + \sum_{i,j} \frac{Z_i Z_j}{R_{ij}} - \sum_{i,j} \frac{Z_i}{|\mathbf{R}_i - \mathbf{r}_j|} + \sum_{i,j} \frac{1}{r_{ij}} \quad (1.40)$$

where P is the momentum of nucleus i , p is the momentum of electron i , Z_i is the nuclear charge of atom i , R_{ij} is the distance between nuclei i and j , and r_{ij} is the distance between electrons i and j . The first two terms are the kinetic energy of the system and the remaining terms are the nucleus-nucleus repulsion, the electron-nucleus attraction, and the electron-electron repulsion energies of the system in that order. A full description of a quantum system must account for all of the above, but due to the large difference in the masses of the nucleus and the electron, the nuclear and electronic terms can be separated into two Hamiltonians. The nuclear Hamiltonian can be written in terms of linear combinations of the nuclear degrees of freedom as

$$H = \sum_{i=1}^N \frac{1}{2}P_i^2 + V(q_i, q_j, \dots, q_N) \quad (1.41)$$

where q_i is the i th linear combination of the nuclear degrees of freedom referred to as the i th normal mode, and $V(q_i, q_j, \dots, q_N)$ is the potential energy as a function of the displacements along the normal modes.

Solving the Schrödinger equation for this vibrational Hamiltonian is made difficult by the complexity of the potential energy function. There are various strategies to approximate the potential energy, including quadrature methods and series expansions. One of the most

popular approximations is the Taylor series expansion of V centered at the minimum-energy geometry written as

$$H = \frac{1}{2!} \sum_{i=1}^N \omega_i (p_i^2 + q_i^2) + \frac{1}{3!} \sum_{ijk}^N \phi_{ijk} q_i q_j q_k + \frac{1}{4!} \sum_{ijkl}^N \phi_{ijkl} q_i q_j q_k q_l + \dots \quad (1.42)$$

where ω_i is the vibrational frequency of mode i , p_i is the momentum associated with vibrational mode i , q_i is the displacement along vibrational mode i and the force constants are defined as

$$\phi_{ijk} = \frac{1}{\sqrt{\omega_i \omega_j \omega_k}} \frac{\partial^3 V}{\partial q_i \partial q_j \partial q_k} \quad (1.43)$$

$$\phi_{ijkl} = \frac{1}{\sqrt{\omega_i \omega_j \omega_k \omega_l}} \frac{\partial^4 V}{\partial q_i \partial q_j \partial q_k \partial q_l}. \quad (1.44)$$

The series expansion has no first-order potential energy term because the forces on all atoms, the first derivative of the potential energy, are zero at the equilibrium geometry. So, the vibrational Hamiltonian's potential energy operator starts with the second-order term, which describes a system of non-interacting harmonic vibrations whose frequencies ω can be computed from the eigenvalues of the second-derivative matrix[19, 20]. The third-derivatives are related to the cubic force constants ϕ_{ijk} and describe the coupling between vibrational modes i , j , and k , while the quartic force constants ϕ_{ijkl} describe the coupling between vibrational modes i , j , k , and l . This potential energy surface is exact only when summed to all orders; however, the effects of the coupling terms generally decrease as one progresses to higher-order terms in the expansion, meaning that it may be safely truncated at an appropriate order based on the desired accuracy. Generally, practical implementations of this series expansion only takes into account up to the semidiagonal quartic force constants which have one repeating index, *i.e.* ϕ_{iijj} , in order to reduce the computational costs. In fact, in the Gaussian 09 implementation of VPT2 [21, 22, 23], the quartic force constants which contribute to the anharmonic correction only includes up to ϕ_{iijj} .

1.2.2 Solutions of the Vibrational Problem

There are a number of methods of solving for the vibrational frequencies of molecules beyond the harmonic (quadratic) potential. Arguably the most accurate method is the vibrational-self consistent field (VSCF)[24, 25, 26] method which is analogous to a mean-field variational solution to the electronic Schrödinger equation, such as the Hartree-Fock method. The VSCF method not only provides a variational wavefunction for the vibrational states of a system, it allows for post-SCF "correlation" methods which allows for coupling between vibrational modes based on the VSCF reference. This is directly analogous to the electronic structure post-SCF correlation methods, such as the vibrational second-order Möller-Plesset perturbation theory (VMP2) [27], degenerate-vibrational perturbation theory[28], and the vibrational configuration interaction methods [29]. An alternative method of special interest for this work is the vibrational second-order perturbation theory (VPT2) [30] based on the harmonic oscillator reference states. This method relies on the harmonic oscillator states as the unperturbed reference state, and as such is subject to large errors for highly-anharmonic potentials. Regardless of the method used for anharmonic corrections, the representation of the potential energy of the system as a function of the vibrational modes has been the primary challenge in obtaining accurate results within reasonable computational costs.

The accuracy of the potential energy term in Equation 1.41 determines the accuracy of the obtained vibrational frequencies, and has been the subject of many studies. One popular representation is the grid-based potential written as a function of the normal mode displacements as

$$V(q_i, q_j, \dots, q_N) = \sum_i V(q_i) + \sum_{i < j} V(q_i, q_j) + \sum_{i < j < k} V(q_i, q_j, q_k) + \dots \quad (1.45)$$

where the potential has been decomposed into the single-mode potential $V(q_i)$, two-mode coupling potential $V(q_i, q_j)$, the three-mode coupling potential $V(q_i, q_j, q_k)$, and so on up to the total number of normal modes. This representation, although accurate, requires electronic structure calculations at each grid point along displacements of all normal modes, then all pairs of normal modes, then all triples and so on up to an impractically large number of calculations. For example, in the GAMESS [31, 32] implementation of the grid-based

VSCF and its correlation corrections, a potential including only up to the two-mode coupling potential requires $Mn + M(M - 1)n^2/2$ number of electronic structure calculations for a system with M number of normal modes and n number of grid points along each normal mode. An alternative to this grid representation is the quartic force-field (QFF)[33] representation, where the Taylor series expansion in Equation 1.42 is truncated at the semidiagonal quartic coupling terms to give

$$V(q_i, q_j, \dots, q_N) = \sum_{ijk}^N \left(\frac{1}{3!} \phi_{ijk} q_i q_j q_k + \frac{1}{4!} \phi_{iijk} q_i^2 q_j q_k \right). \quad (1.46)$$

The third and fourth derivatives of the energy with respect to the normal mode displacements can be obtained from analytically or numerically differentiating the Hessian (second derivative) matrix, resulting in $6(M + M(M - 1))$ electronic structure calculations for a system of M normal modes. For systems with large cubic couplings and small semidiagonal quartic couplings, this representation dramatically reduces the number of electronic structure calculations with minor reduction in accuracy. It is for this reason that the VPT2 method uses the QFF potential.

In second-order vibrational perturbation theory, the Hamiltonian in Equation 1.41 is truncated at the fourth-order terms with one repeating index as

$$H = \frac{1}{2!} \sum_{i=1}^N \omega_i (p_i^2 + q_i^2) + \sum_{ijk}^N \left(\frac{1}{3!} \phi_{ijk} q_i q_j q_k + \frac{1}{4!} \phi_{iijk} q_i^2 q_k q_l \right). \quad (1.47)$$

The harmonic part of the Hamiltonian is taken as the unperturbed Hamiltonian $H^{(0)}$ while the cubic and quartic coupling terms are taken as the perturbation to the harmonic system. The standard Rayleigh-Schrödinger perturbation theory (RSPT) can be applied to the resulting nuclear Schrödinger equation in the space of products of the normal mode wavefunctions. The first-order wavefunction which gives the second-order vibrational frequencies can be written as

$$|i\rangle = |i^{(0)}\rangle + |i^{(1)}\rangle \quad (1.48)$$

for arbitrary state i and an arbitrary number of vibrational modes. Then an effective vibrational Hamiltonian can be written as

$$\langle i|H_{\text{eff}}|i\rangle = \langle i^{(0)}|\sum_{ijk}^N \frac{1}{3!}\phi_{ijk}q_i^2q_jq_k|i^{(0)}\rangle + \langle i^{(0)}|\sum_{ijk}^N \frac{1}{4!}\phi_{ijk}q_iq_jq_k|i^{(1)}\rangle + \langle i^{(1)}|\sum_{ijk}^N \frac{1}{4!}\phi_{ijk}q_iq_jq_k|i^{(0)}\rangle \quad (1.49)$$

whose energies are

$$\langle i|H_{\text{eff}}|i\rangle = \chi_0 + \sum_i^N \omega_i \left(i + \frac{1}{2}\right) + \sum_{i \geq j} \chi_{ij} \left(i + \frac{1}{2}\right) \left(j + \frac{1}{2}\right). \quad (1.50)$$

Then the transition frequencies of the fundamentals ν_i , overtones ν_{2i} , and combination bands ν_{ij} can be computed as

$$\nu_i = \omega_i + 2\chi_{ii} + \frac{1}{2} \sum_{j \neq i} \chi_{ij}, \quad (1.51)$$

$$\nu_{2i} = 2\nu_i + 2\chi_{ii}, \quad (1.52)$$

$$\nu_{ij} = \nu_i + \nu_j + \chi_{ij}, \quad (1.53)$$

where χ_{ii} and χ_{ij} are the diagonal and off-diagonal anharmonicity constants defined as

$$\begin{aligned} \chi_{ii} &= \frac{1}{16} \left[\phi_{iiii} - \sum_j^N \phi_{iij}^2 \frac{8\omega_k^2 - 3\omega_j^2}{\omega_j(4\omega_i^2 - \omega_j^2)} \right] \\ \chi_{ij} &= \frac{1}{4} \left\{ \phi_{iijj} - \sum_k^N \phi_{iik} \phi_{kjj} \frac{1}{\omega_k^2} + \right. \\ &\quad \left. + \sum_k^N \phi_{ijk}^2 \frac{2\omega_k(\omega_i^2 + \omega_j^2 - \omega_k^2)}{(\omega_i + \omega_j + \omega_k)(\omega_i - \omega_j + \omega_k)(\omega_i + \omega_j - \omega_k)(\omega_i - \omega_j - \omega_k)} \right\}. \end{aligned} \quad (1.54)$$

The analytical anharmonic constants are derived from the second-order RSPT sum over states with the integrals evaluated using the ladder operator formalism. The force constants are calculated by numerically differentiating the Hessian once for the cubic force constants and twice for the quartic force constants. For a system of N atoms, the VPT2 method requires $6N - 11$ Hessian matrix calculations in order to obtain the required force constants. Due to this favorable scaling relative to the variational methods, the VPT2 method will be the primary computational tool for the work described in Chapter 4.

2.0 APPLICATION OF ELECTRONIC STRUCTURE METHODS TO COUPLED DRUDE OSCILLATORS

The work described in this chapter was adapted from Reference [34] and draws from the theoretical foundations of the quantum Drude oscillator model described in Chapter 1, Section 1.1 and the intermolecular interactions described in Section 1.1.4. I would like to acknowledge the support and guidance of Dr. Vamsee Voora, and discussions with Dr. Filipp Furche and Dr. Andreas Hesselmann on the matter of the random-phase approximation. This work was supported by the National Science Foundation’s CHE1362334 grant, and the computational resources at the University of Pittsburgh’s Center for Simulation and Modeling.

2.1 INTRODUCTION

The system of two Drude oscillators, separated by a distance R , interacting via a dipole-dipole coupling is a textbook model for explaining the origin of the C_6R^6 dispersion interaction between two atoms or molecules[35]. The dispersion interaction between the two oscillators can be solved analytically by a change of variables. Here, we find it instructive to apply standard electronic structure methods including RayleighSchrodinger perturbation theory[36], configuration interaction (CI), coupled cluster doubles (CCD) theory[37, 38], and the random phase approximation (RPA)[39, 40, 41] to calculate the interaction energy between two Drude oscillators. The configurations used in the calculations are represented in terms of products of harmonic oscillator functions. Our analysis shows that while the CI and CCD methods require including excitations into all excited levels to obtain the exact interaction energy, the RPA method gives the exact answer, allowing only excitations into

the first excited state of each oscillator. The insensitivity of the RPA result to the basis set is explained in terms of the Hamiltonian being quadratic in nature.

2.2 METHODOLOGY

The Hamiltonian for the model system is given by

$$H = -\frac{1}{2}\frac{d^2}{dx_1^2} - \frac{1}{2}\frac{d^2}{dx_2^2} + \frac{1}{2}kx_1^2 + \frac{1}{2}kx_2^2 - \frac{2q^2x_1x_2}{R^3} \quad (2.1)$$

where for simplicity, we assume one-dimensional oscillators and employ atomic units. We have further assumed the mass associated with the oscillator is equal to that of the electron, which is one in atomic units. We recast H as:

$$H = H_0 + V \quad (2.2)$$

where H_0 is the Hamiltonian for the non-interacting oscillators and the perturbation V is defined as

$$V = -\frac{2q^2x_1x_2}{R^3} = \gamma x_1x_2. \quad (2.3)$$

With the change of variables

$$\mu = \frac{1}{\sqrt{2}}(x_1 + x_2) \quad (2.4)$$

and

$$\nu = \frac{1}{\sqrt{2}}(x_1 - x_2) \quad (2.5)$$

H separates to give two non-interacting harmonic oscillators with frequencies

$$\omega_1 = \omega\sqrt{1 - \frac{\gamma}{k}} \quad (2.6)$$

and

$$\omega_2 = \omega\sqrt{1 + \frac{\gamma}{k}}, \quad (2.7)$$

where ω is the frequency of an unperturbed oscillator. The change in zero-point energy of the system due to the interaction between the oscillators is

$$E_{\text{int}} = \frac{\omega}{2} \left(-2 + \sqrt{1 - \frac{\gamma}{k}} + \omega \sqrt{1 + \frac{\gamma}{k}} \right). \quad (2.8)$$

Taylor series expansion of the square roots gives

$$E_{\text{int}} = -\frac{\omega\gamma^2}{8k^2} - \frac{5\omega\gamma^4}{128k^4} - \dots \quad (2.9)$$

through the first two non-zero terms. This can be rewritten as

$$E_{\text{int}} = -\frac{1}{2}\alpha^2 \frac{\omega}{R^6} - \frac{5}{8}\alpha^4 \frac{\omega}{R^{12}} \quad (2.10)$$

where use was made of the fact that the polarizability, α , of a Drude oscillator is q^2/k . The first term is the well-known London expression for the leading dispersion interaction between two atoms or molecules[42].

2.3 APPLICATIONS OF ELECTRONIC STRUCTURE METHODS TO THE DRUDE OSCILLATOR PROBLEM

We now apply various electronic structure methods to the Hamiltonian given by Equation 2.1. The basis set is taken to be products of harmonic oscillator functions $|ij\rangle$, where i and j specify the quantum numbers of the oscillators 1 and 2, respectively.

$$\begin{array}{c|cccccc}
& |00\rangle & |11\rangle & |20\rangle & |02\rangle & |22\rangle & \dots \\
\langle 00| & \omega & \delta & 0 & 0 & 0 & \dots \\
\langle 11| & \delta & 3\omega & \sqrt{2}\delta & \sqrt{2}\delta & 2\delta & \dots \\
\langle 20| & 0 & \sqrt{2}\delta & 3\omega & 0 & 0 & \dots \\
\langle 02| & 0 & \sqrt{2}\delta & 0 & 3\omega & 0 & \dots \\
\langle 22| & 0 & 2\delta & 0 & 0 & 5\omega & \dots \\
\vdots & \vdots & \vdots & \vdots & \vdots & \vdots & \ddots
\end{array}$$

2.3.1 Configuration interaction, Rayleigh-Schrödinger perturbation theory, and CCD

The CI matrix for the ground state of the coupled oscillator problem assumes the form where $\delta = \gamma/(2\omega)$. As seen from the CI matrix the configurations that contribute to the ground state wave function are $|00\rangle$, $|11\rangle$, $|20\rangle$, $|02\rangle$, $|22\rangle$, etc. Note that the $|00\rangle$ configuration mixes directly only with $|11\rangle$. If only the $|00\rangle$ and $|11\rangle$ configurations are retained, the energy is

$$2\omega - \omega\sqrt{1 + \frac{\delta^2}{\omega^2}} = \omega - \frac{\delta^2}{8\omega^3} + \frac{\delta^4}{8\omega^3} - \dots = \omega - \frac{\omega\gamma^2}{8k^2} + \frac{\omega\gamma^4}{128k^4} - \dots \quad (2.11)$$

which is correct only through the leading correction, *i.e.*, the second-order perturbation theory result. In fact, the $O(\gamma^4)$ term enters with the wrong sign. As is clear from the structure of the CI matrix, the $|20\rangle$, $|02\rangle$, and $|22\rangle$ configurations must also be included to obtain the energy correct through fourth-order perturbation theory. There are four contributions to the fourth-order energy:

$$\begin{aligned}
E^{(4)} = & \frac{\langle 00|V|11\rangle \langle 11|V|22\rangle \langle 22|V|11\rangle \langle 11|V|00\rangle}{\left(E_{|00\rangle}^{(0)} - E_{|11\rangle}^{(0)}\right)^2 \left(E_{|00\rangle}^{(0)} - E_{|22\rangle}^{(0)}\right)} + \\
& + \frac{\langle 00|V|11\rangle \langle 11|V|20\rangle \langle 20|V|11\rangle \langle 11|V|00\rangle}{\left(E_{|00\rangle}^{(0)} - E_{|11\rangle}^{(0)}\right)^2 \left(E_{|00\rangle}^{(0)} - E_{|20\rangle}^{(0)}\right)} + \\
& + \frac{\langle 00|V|11\rangle \langle 11|V|02\rangle \langle 02|V|11\rangle \langle 11|V|00\rangle}{\left(E_{|00\rangle}^{(0)} - E_{|11\rangle}^{(0)}\right)^2 \left(E_{|00\rangle}^{(0)} - E_{|02\rangle}^{(0)}\right)} - \\
& - \frac{\langle 00|V|11\rangle \langle 11|V|00\rangle \langle 00|V|11\rangle \langle 11|V|00\rangle}{\left(E_{|00\rangle}^{(0)} - E_{|11\rangle}^{(0)}\right)^3}
\end{aligned} \quad (2.12)$$

The terms involving $|20\rangle$, $|02\rangle$, and $|22\rangle$ each contribute $-\delta^4/4\omega^3$, and the last term corresponding to the disconnected diagram contributes $\delta^4/8\omega^3$. Figure 2.1 reports the interaction energy vs. distance for the coupled Drude oscillator problem in the case $k = 0.04$ a.u., $q = 1$ a.u., and $m = 1$ a.u. (This corresponds to an oscillator excitation energy of about 5.4 eV.) Results are reported for three different CI calculations: the smallest including only the $|00\rangle$ and $|11\rangle$ configurations, the intermediate including the $|00\rangle$, $|11\rangle$, $|20\rangle$, $|02\rangle$, $|22\rangle$ configurations, and the largest including the $|00\rangle$, $|11\rangle$, $|20\rangle$, $|02\rangle$, $|22\rangle$, $|13\rangle$, $|31\rangle$, and $|33\rangle$ configurations. Over the range of R values considered ($4 \leq R \leq 6$ a.u.) the largest CI calculation gives interaction energies essentially indistinguishable from the exact values, while the results from the intermediate size CI calculations differ slightly from the exact result for $R \leq 4.5$ a.u. On the other hand, the energies from the small CI calculations differ appreciably from the exact result for R values less than about 5 a.u. For the two-Drude oscillator model system, the CCD method[36, 37] gives the same result as the CI calculations, when using the same configuration space. For this reason, the CCD method is not pursued further.

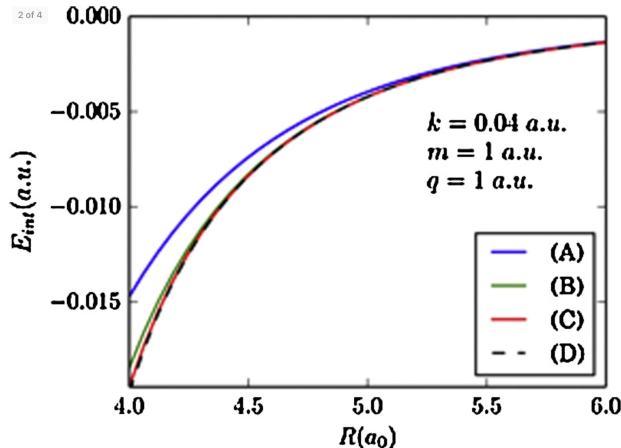


Figure 2.1: Interaction energy of two Drude oscillators coupled through the dipole-dipole interaction calculated with the basis (A) $|00\rangle, |11\rangle$; (B) $|00\rangle, |11\rangle, |20\rangle, |02\rangle, |22\rangle$; (C) $|00\rangle, |11\rangle, |20\rangle, |02\rangle, |22\rangle, |13\rangle, |31\rangle, |33\rangle$, compared to (D) the exact interaction energy.

2.3.2 The Random-Phase Approximation

As is well known the random-phase approximation (RPA) equations can be written as

$$\begin{pmatrix} \mathbf{A} & \mathbf{B} \\ -\mathbf{B} & -\mathbf{A} \end{pmatrix} \begin{pmatrix} \mathbf{x} \\ \mathbf{y} \end{pmatrix} = E \begin{pmatrix} \mathbf{I} & 0 \\ 0 & \mathbf{I} \end{pmatrix} \begin{pmatrix} \mathbf{x} \\ \mathbf{y} \end{pmatrix} \quad (2.13)$$

where the \mathbf{A} matrix includes interactions between various single excitations and the \mathbf{B} matrix accounts for the mixing of double excitations with the reference configuration[39, 40, 41]. Due to the nature of the RPA equations, the only configurations that are important for the correlation energy for the model considered here are $|10\rangle$ and $|01\rangle$.

The entries in the \mathbf{A} matrix are $\langle 10|H - E_0|10\rangle = \langle 01|H - E_0|01\rangle = \omega$ and $\langle 10|H - E_0|01\rangle = \delta$, while the non-zero entries in the \mathbf{B} matrix are $\langle 11|H|00\rangle = \langle 00|H|11\rangle = \delta$. Thus, the \mathbf{A} and \mathbf{B} matrices are

$$\mathbf{A} = \begin{pmatrix} \omega & \delta \\ \delta & \omega \end{pmatrix}, \mathbf{B} = \begin{pmatrix} 0 & \delta \\ \delta & 0 \end{pmatrix}, \quad (2.14)$$

and the relevant excitation energies are

$$E_1 = \omega \sqrt{1 + \frac{2\delta}{\omega}} \quad (2.15)$$

and

$$E_2 = \omega \sqrt{1 - \frac{2\delta}{\omega}}. \quad (2.16)$$

Several different strategies have been developed for extracting ground state correlation energies of systems where the electrons are treated explicitly[40, 43, 44, 45, 46]. For the Drude oscillator problem, the logical choice is to use

$$E_{\text{int}} = \frac{1}{2} \sum_{i=1} (\omega_i^{\text{RPA}} - \omega_i^{\text{TDA}}), \quad (2.17)$$

where TDA refers to the Tamm-Dancoff approximation which retains only the \mathbf{A} matrix in Equation 2.13. For the coupled Drude oscillator problem with only $|0\rangle \rightarrow |1\rangle$ excitations of the individual oscillators, this gives

$$E_{\text{int}} = \frac{\omega}{2} \left(-2 + \sqrt{1 + \frac{2\delta}{\omega}} + \sqrt{1 - \frac{2\delta}{\omega}} \right), \quad (2.18)$$

which is identical to the exact solution given by Equation 2.8. At first sight, this is a surprising result, since obtaining the exact correlation energy with the CI or CCD methods requires inclusion of all configurations $|ij\rangle$, where $|i+j|$ is an even integer. It is also interesting in light of the fact that it has been shown that the direct RPA method is equivalent to the ring CCD method (without exchange) for estimating the correlation energy of a many-electron system[47, 48, 49].

Comparison of Equations 2.15 and 2.16 with Equations 2.6 and 2.7 reveals that the RPA method allowing only $|0\rangle \rightarrow |1\rangle$ excitations of the oscillators gives the exact excitation energies of the coupled Drude oscillator problem. It is for this reason that Equation 2.17 gives the exact value for the ground state correlation energy when using the restricted excitation space. This raises the question as to the structure of the \mathbf{A} and \mathbf{B} matrices when excitations into levels $|2\rangle$, $|3\rangle$, etc., are allowed. In this case, the eigenvalues of the \mathbf{A} matrix become $n\omega$ where n is the quantum number of the excitation. Moreover, the fact that the RPA excitation energies are exact when allowing only $|0\rangle \rightarrow |1\rangle$ excitations of the oscillators follows from the quadratic form of the Hamiltonian as can be seen from the derivation of the RPA equations by Rowe[50]. Additionally, we note that the fact that the RPA method gives the exact correlation energy for harmonic oscillators coupled through the dipole-dipole interaction, has been demonstrated by Tkatchenko and co-workers[5] by use of the adiabatic connection fluctuation-dissipation theorem (AC-FDT)[6]. Although Tkatchenko et al. did not explicitly introduce a basis set in their treatment, they did employ the fact that the functional form of the frequency-dependent dipole polarizability of a Drude oscillator has a single pole, consistent with the contribution of only the $|0\rangle \rightarrow |1\rangle$ transition. If the Hamiltonian were extended to include also dipole-quadrupole and quadrupole-quadrupole coupling, $|0\rangle \rightarrow |2\rangle$ excitations would also enter into the RPA equations, and the method would no longer give the exact excitation energies nor the exact ground state energy. Examination of the Goldstone diagrams for the RPA correlation energy reveals that at all orders other than second all diagrams contributing to the energy are exclusion principle violating (EPV) in nature. This is illustrated in Figure 2.2, which displays one of the fourth-order contributions to the energy. This is in contrast to the RSPT result for which the negative contributions to the correlation energy are non-EPV in nature and include excitations into $|20\rangle$, $|02\rangle$, and $|22\rangle$.

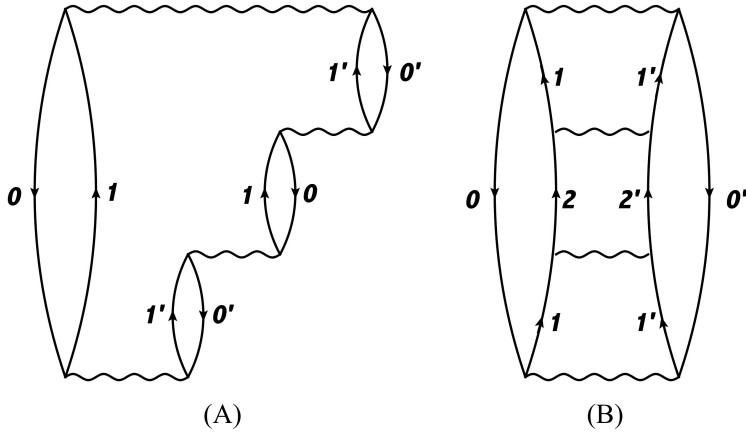


Figure 2.2: (A) Fourth-order exclusion principle violating interaction diagram appearing in the RPA. $|0\rangle$ and $|1\rangle$ correspond to oscillator 1, while $|0'\rangle$ and $|1'\rangle$ correspond to oscillator 2. (B) Shows a fourth-order contribution to the RSPT involving excitation into the $|22\rangle$ level.

2.4 CONCLUSION

Quantum Drude oscillators have proven to be a valuable approach for describing dispersion interactions in molecules, clusters, and solids as well as at interfaces. In this work the interaction energies for a pair of interacting quantum Drude oscillators with dipole-dipole coupling is calculated using the perturbation theory, CI, CCD, and RPA methods. The RPA method is shown to give the exact excitation energies and the exact correlation energy of the ground state of the coupled Drude oscillator problem when allowing only $|0\rangle \rightarrow |1\rangle$ excitations of the oscillators. This lack of sensitivity to the basis set (and, hence, excitation level) is a consequence of the Hamiltonian including only dipole-dipole coupling of the oscillators. It also follows from the result of Tkatchenko and coworkers who showed using the AC-FDT that the RPA gives the exact interaction energy for a system of oscillators interacting through dipole-dipole coupling.

3.0 DISPERSION DIPOLES FOR COUPLED DRUDE OSCILLATORS

This work was adapted from Reference [51] and builds on the Drude oscillator description of the dispersion interaction described in Chapter 2. As with the previous chapter, Dr. Vamsee Voora contributed to this work through valuable discussions. This work was funded by the National Science Foundation’s CHE1362334 grant and the Pittsburgh Quantum Institute’s Graduate Student Grant, and computational resources were provided by the University of Pittsburgh’s Center for Simulation and Modeling.

3.1 INTRODUCTION

Long-range dispersion interactions between atoms or molecules are generally explained in terms of correlated charge fluctuations of the two atoms (or molecules)[18]. The simplest wave-function approach that accounts for dispersion is second-order Mller-Plesset perturbation theory (MP2)[52]. In this picture, the dispersion interaction results from the interaction of fluctuating dipoles of the two atoms or molecules. In contrast, in the last paragraph of Feynman’s classic 1939 paper, he observed that the long-range dispersion interaction between two spherical atoms causes each atom to acquire a permanent dipole moment with the negative ends of the two dipoles pointed toward each other[53]. Feynman stated:

Van der Waal’s forces can also [*sic*] be interpreted as arising from charge distributions with higher concentration between the nuclei. The Schrödinger perturbation theory for two interacting atoms at a separation R , large compared to the radii of the atoms, leads to the results that the charge distribution of each is distorted from central symmetry, a dipole moment of order $1/R^7$ being induced in each atom. The negative charge distribution of each atom has its center of gravity moved slightly toward the other. It is not the interaction of these dipoles which leads to van der Waals’ force, but rather the attraction of each nucleus

for the distorted charge distribution of its *own* electrons that gives the attractive $1/R^7$ force.

The dipole on each atom and the force on the nuclei resulting from the charge distortion display a R^{-7} dependence on the separation of the atoms[53, 54, 55]. Feynman further observed that one can obtain the dispersion energy from a classical electrostatic calculation involving the altered charge distributions of the atoms. Eliason and Hirschfelder[56] confirmed numerically the existence of the R^{-7} dispersion force for two interacting H atoms in their S ground states, while Byers Brown and Whisnant[57] confirmed the existence of dispersion dipoles. Hunt showed, through a non-linear response approach, that the dispersion-induced dipole on one atom (or molecule) results from the interaction of its dipole-dipole-quadrupole polarizability with the instantaneous dipole on the other atom (or molecule)[58]. This approach was exploited in references[59, 60, 61]. Hunt also presented an analytical proof of Feynmans conjecture about the dispersion force for interacting atoms in S states, and generalized it to molecules of arbitrary symmetry[62]. She has also been able to reconcile the two seemingly different views of dispersion[62]

In the present article, we analyze the dispersion-induced dipole for the case of two interacting quantum Drude oscillators[63]. In doing so, we draw on the work of Linder and Kromhout[60] and Galatry and Gharbi[61]. The latter authors have already published the expression for the dispersion dipole for two interacting 3D Drude oscillators, which they obtained using a response-function approach. In the present study, we report the second-order wavefunction that gives the dispersion dipoles of the interacting oscillators and use it to obtain the dispersion-induced changes in the charge distribution. We also confirm that one can obtain the C_6 coefficient for the interacting Drude oscillators from the electrostatic force resulting from the altered charge distributions.

3.2 THEORY

The problem of two quantum Drude oscillators with dipole-dipole coupling is a textbook model for illustrating the origin of the long-range C_6/R^6 dispersion interaction[64]. Here,

R is the distance between the two oscillators, and C_6 is the dispersion coefficient associated with the R^{-6} contribution. However, when only dipole-dipole coupling is allowed, this model does not give rise to the permanent dipoles predicted by Feynman. To recover the permanent dipoles induced by dispersion it is necessary to include dipole-quadrupole coupling.

In this work, we assume that the two oscillators lie on the z -axis, and, for simplicity, we initially assume that oscillator A only has charge fluctuations in the z -direction and that the coupling with oscillator B is through the $-2q^2 z_1 z_2 / R^3$ and $2q^2 z_1 \theta_2^{zz} / R^4$ terms, where $\theta^{zz} = (3z^2 r^2) / 2$. In this case, the relevant wave function through second-order (in atomic units) becomes

$$\begin{aligned} \psi = & |00\rangle + \frac{2q^2}{R^3} \frac{\langle 00 | z_1 z_2 | 11 \rangle}{2\omega_0} |11\rangle - \frac{2q^2}{R^4} \frac{\langle 00 | (3z^2 r^2) / 2 | 12 \rangle}{2\omega_0} |12\rangle - \\ & - \frac{4q^4}{R^7} \frac{\langle 00 | z_1 z_2 | 11 \rangle \langle 11 | (3z^2 r^2) / 2 | 01 \rangle}{2\omega_0^2} |01\rangle - \frac{4q^4}{R^7} \frac{\langle 00 | (3z^2 r^2) / 2 | 12 \rangle \langle 12 | z_1 z_2 | 01 \rangle}{2\omega_0^2} |01\rangle, \end{aligned} \quad (3.1)$$

where in configuration $|ij\rangle$, i and j specify the states of oscillators A and B , respectively, and ω_0 is the frequency of the Drude oscillator. $|0\rangle$, $|1\rangle$, and $|2\rangle$ denote the ground and first two excited states of the one-dimensional Drude oscillator. In Equation 3.1 we have left out the terms that do not contribute to the dipole on oscillator B . Figure 3.1 shows the dispersion-induced change in the charge density for the wavefunction in Equation 3.1 extended to also include the distortion on oscillator A caused by the fluctuation in the z -direction of the charge distribution on oscillator B . The oscillators are separated by $R = 12 a_0$, and the parameters are chosen to be $q = 0.5$ a.u., $m = 1$ a.u., and $k = 0.16$ a.u., resulting in $\alpha = 1.56$ a.u.³ = 0.23 \AA^3 and $\omega_0 = 0.40$ a.u., values roughly appropriate for He. As seen from this figure each oscillator acquires a permanent dipole with the negative ends of the dipoles pointing towards each other just as Feynman predicted for interacting atoms. Using the wave function in Equation 3.1, the dipole moment of oscillator B is calculated to be (retaining terms through R^{-7})

$$\mu_B = -\frac{2q^5}{km^2\omega_0^3 R^7} = -\frac{\alpha_A B_B^{zzzz}\omega_0}{R^7} = -\frac{2\alpha_A \alpha_B}{m\omega_0 R^7} \quad (3.2)$$

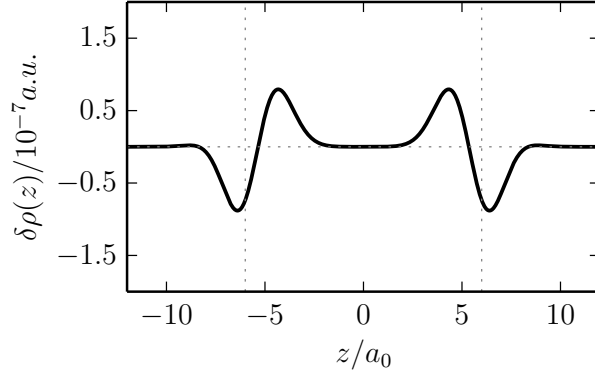


Figure 3.1: Dispersion-induced change in the charge densities of two interacting one-dimensional Drude oscillators at a distance of $12 a_0$ and with $k = 0.16$ a.u., $q = 0.5$ a.u., and $m = 1$ a.u.

where α_A and α_B are the static dipole polarizabilities of A and B , which are equal to q^2/k , m is the mass associated with an oscillator, and B_B^{zzzz} is the $zzzz$ component of the static dipole-dipole-quadrupole hyperpolarizability of B , which is equal to $2q^3/m^2\omega_0^4$ for a Drude oscillator. This latter result was derived from Eq. A4 of reference [60]. The charge displacements in Figure 3.1 have both dipolar and quadrupolar contributions, the latter of which results from the R^{-6} dipole-dipole coupling. The distortion due to dipole-dipole coupling alone is shown in Figure 3.2. The induced dipole on B due to the fluctuation on A can also be expressed in terms of the integral of the product of the frequency-dependent dipole polarizability of A and the frequency-dependent dipole-dipole-quadrupole hyperpolarizability evaluated at imaginary frequency [59, 60, 61, 62].

$$\mu_B^z = \frac{1}{3\pi} \int_0^{\text{inf}} B_{z\alpha\beta\gamma}(-i\omega, i\omega) \alpha_A^{\delta\epsilon}(-i\omega) T_{\alpha\delta} T_{\epsilon\beta\gamma} d\omega \quad (3.3)$$

where $T_{\alpha\delta}$ and $T_{\epsilon\beta\gamma}$ are the standard dipole-dipole and dipole-quadrupole coupling tensors, respectively. Bishop and Pipan have reported accurate values of $\alpha(i\omega)$ and $B(-i\omega, i\omega)$ for

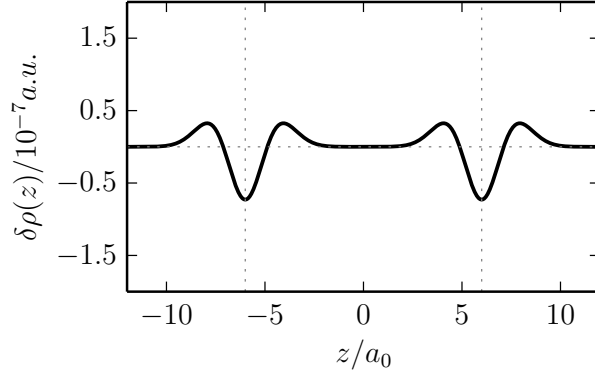


Figure 3.2: The quadrupolar charge distortion due to dipole-dipole coupling of two one-dimensional Drude oscillators at a separation of $12 a_0$ and with the parameters as used in Figure 3.1.

H, He, and H_2 as a function of ω [65]. For the simplified 1D model described above, one need only to consider $\alpha^{zz}(i\omega)$ and $B^{zzzz}(-i\omega, i\omega)$ which are given by

$$\alpha^{zz}(i\omega) = \alpha^{zz}(0) \frac{\omega_0^2}{\omega^2 + \omega_0^2} \quad (3.4)$$

and

$$B^{zzzz}(-i\omega, i\omega) = B^{zzzz}(0) \frac{\omega_0}{\omega^2 + \omega_0^2} \quad (3.5)$$

where the latter result was obtained from Eq. A4 of Linder and Kromhauht [60]. Interestingly, the frequency dependence of B^{zzzz} is even simpler for the Drude oscillator than obtained using closure relations as used by these authors. Using these expressions to evaluate the integral in Equation 3.3 gives the same expression for the dipole moment as was obtained from the perturbation theory wave function (Equation 3.2). For the simplified 1D model considered above, the force on the fixed charge of oscillator B , obtained by use of the electrostatic Hellmann-Feynman theorem, is

$$F_B = -k \langle z_2 \rangle = -\frac{k \alpha_A^{zz}(0) B_B^{zzzz}(0)}{q R^7} \quad (3.6)$$

which is also equal to $-6C_6/R^7$. This gives the result $C_6 = \alpha^2\omega_0/3$, compared to the exact result of $\alpha^2\omega_0/2$ for the C_6 value for 1D Drude oscillators [61]. This discrepancy is simply a consequence of our neglect in the simplified treatment of contributions of B_B^{zzxx} and B_B^{zzyy} in response to the fluctuation of the charge density of A in the z direction. When these are included, the correct value of C_6 is obtained for the 1D case.

In three dimensions, the Hamiltonian for two interacting Drude oscillators has the form

$$\hat{H} = H_A^{(0)} + H_B^{(0)} - T_{\alpha\beta}\mu_\alpha^A\mu_\beta^B - \frac{1}{3}(T_{\alpha\beta\gamma}\mu_\alpha^A\theta_{\beta\gamma}^B - T_{\alpha\beta\gamma}\theta_{\alpha\beta}^A\mu_\gamma^B) \quad (3.7)$$

where $H_A^{(0)}$ and $H_B^{(0)}$ are the Hamiltonians for the non-interacting oscillators, and the standard Einstein summation notation is used. μ_α^I and $\theta_{\alpha\beta}^I$ are the dipole and quadrupole moment operators for oscillator I . The resulting wave function through second-order contains three R^{-3} , 10 R^{-4} , and 34 R^{-7} terms. Using this to evaluate gives

$$\mu_B^z = -\frac{9q^5}{2m^3\omega_0^5R^7} = -\frac{9}{2}\alpha_A\alpha_B\frac{1}{m\omega_0R^7} = -\frac{9}{4}\alpha_A B_B^{zzzz}\frac{\omega_0}{R^7} \quad (3.8)$$

In the evaluation of Equation 3.8 the product of the R^{-3} and R^{-4} terms contributes 1/6 of the dipole moment while the R^{-7} terms contribute 5/6. In comparison, Hirschfelder and Eliason found that 93% of the contributions to the dipole moment arise from the R^{-7} terms for the case of two hydrogen atoms[56]. We note that Levine also considered the dispersion dipole for interacting Drude oscillators[66]. However, due to the approximations that he made in averaging the interactions, the resulting dispersion dipole is 10/3 times larger than that reported in Equation 3.8. In treating the interacting 3D Drude oscillators, using the response function approach, it is necessary to consider seven components of B , B^{zzzz} , B^{zzxx} , B^{zzyy} , B^{zzxz} , B^{zyyz} , B^{zxzx} , and B^{zyzy} , which are related as follows[58, 60]:

$$\begin{aligned} B^{zzxx} &= B^{zzyy} = -\frac{1}{2}B^{zzzz}, \\ B^{zzxz} &= B^{zyyz} = \frac{3}{4}B^{zzzz}, \\ B^{zxzx} &= B^{zyzy} = \frac{3}{4}B^{zzzz}. \end{aligned} \quad (3.9)$$

Allowing for these relations, the net dispersion dipole on oscillator B can be expressed as

$$\mu_B^z = -\frac{9}{\pi R^6} \int_0^{\text{inf}} \alpha_A^{zz}(i\omega) B_B^{zzzz}(-i\omega, i\omega), \quad (3.10)$$

where α_A^{zz} and $(i\omega)B_B^{zzzz}(-i\omega, i\omega)$ are defined above in Equations 3.4 and 3.5. Evaluation of the integral gives the same result for the dipole induced on oscillator B as obtained from the perturbation theory approach (Equation 3.8). Moreover, for the 3D Drude oscillator case the value of C_6 evaluated using the electrostatic Hellmann-Feynman theorem is which is the exact value of the C_6 coefficient for two interacting 3D Drude oscillators as evaluated using second-order perturbation theory. In Figure 3.3, we display a contour plot of the dispersion-induced changes in the charge distribution of two interacting 3D Drude oscillators separated by $R = 12 a_0$, and with the same parameters as used in the 1D case above.

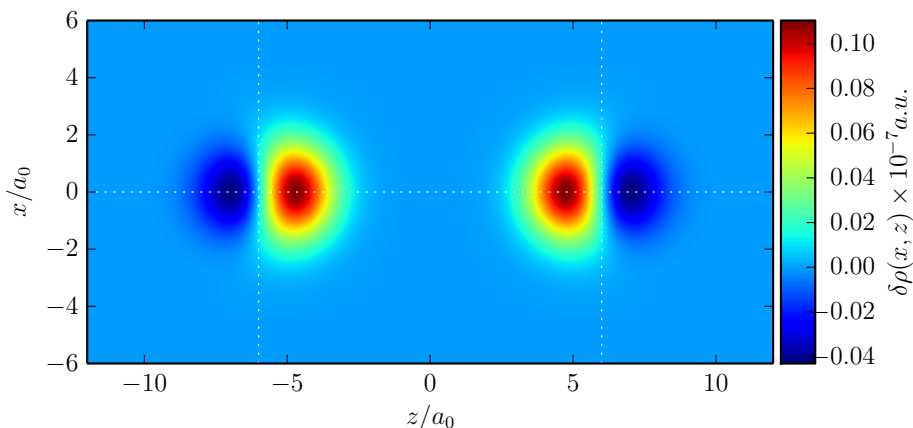


Figure 3.3: Dispersion-induced change in the charge densities of two interacting 3D Drude oscillators separated by a distance of $12 a_0$ and with the parameters specified in the text.

3.3 CONCLUSIONS

In this work we derive, using both perturbation theory and a response function approach, the expression for the dispersion-induced dipoles of interacting Drude oscillators. We also derive the C_6 dispersion coefficient from the electrostatic Hellmann-Feynman theorem. As noted in previous studies of H_2 and He_2 at interatomic distances beyond the overlap region[67, 68, 69], the permanent dipoles resulting from the dispersion interactions are very small. Due to

the small values of these dipoles, it has been concluded by some researchers, that it is essential to use variational (or, at least coupled-cluster) approaches to accurately predict the dipoles when dealing with atomic or molecule systems. Although, one has to be careful in extrapolating from the Drude model to real atoms or molecules, our results suggest that even the second-order Rayleigh-Schrodinger perturbation theory wavefunction should suffice for calculating the dispersion-induced dipoles.

In recent years, several methods of correcting density-functional theory for dispersion that involve distortions of the atomic charges have been introduced. These include the dispersion-corrected atom-centered potential approach (DCACP)[70, 71] the density displacement model of Hesselmann[72], and the self-consistent Tkatchenko-Scheffler[73] model of Ferri and co-workers[74]. However, the success of these models at describing dispersion interactions appears to be unrelated to the electrostatic Hellmann-Feynman approach for obtaining the C_6 coefficient from the charge distortion. This concludes the Drude oscillator portion of this thesis.

4.0 FIELD-EFFECT ORIGINS OF THE HYDRATION-INDUCED SHIFTS OF THE VIBRATIONAL SPECTRAL SIGNATURES OF THE HYDRONIUM ION IN GAS-PHASE PROTONATED WATER CLUSTERS

This work was adapted from References [75] and [76], and details my contributions to the study of proton accommodation in gas-phase water clusters $\text{H}^+(\text{H}_2\text{O})_{n=2-28}$, with the necessary theoretical background described in Section 1.1. The experimental vibrational spectra were collected by Joseph A. Fournier, Conrad T. Wolke, and Mark A. Johnson at the Sterling Chemistry Laboratory, Yale University. Shawn M. Kathmann and Sotiris S. Xantheas contributed to this work through the calculation of the electric field lines in the clathrate cage cluster $\text{H}^+(\text{H}_2\text{O})_{21}$. My contributions were supported by the U.S. Department of Energy under Grant No. DE-FG02-06ER15066, and utilized the computational resources at the University of Pittsburgh’s Center for Simulation and Modeling. Calculations were performed using the Gaussian 09 suite of programs [21]. Harmonic calculations were performed at both the B3LYP/6-31+G(d) and B3LYP/aug-cc-pVTZ level of theory. Anharmonic VPT2 calculations [22, 23] were performed at the B3LYP/6-31+G(d) level for the $n = 1, 3, 4, 5, 10$, and 21 clusters. The decomposition of the intermolecular interaction energies was performed using symmetry-adapted perturbation theory [77, 78] in the SAPT2 approximation [79, 80] using the PSI4 code [81]. The 1D potential energy curves of the hydronium OH stretching coordinate were done at the B3LYP/6-31+G(d) level of theory.

4.1 INTRODUCTION

In spite of the fact that acid-base behavior lies at the foundation of aqueous chemistry, the fundamental cationic species created when an Arrhenius acid releases a proton into water has proven remarkably difficult to capture at the molecular level[82, 83, 84, 85, 86, 87, 88]. The complexity arises from the fact that the excess proton can be associated with a single water molecule, thereby becoming indistinguishable from the original OH bonds of that water molecule, or it may be delocalized between two water molecules. When this process occurs in bulk water, it results in a charge defect that is manifested through distortions in the proximal hydrogen bonding network. The spectroscopic characterization of the molecular entity that carries the excess charge in water is hampered by the fact that the vibrational spectrum corresponding to the OH stretching motions in pure water extends over hundreds of wavenumbers[86, 89, 90, 91]. Attempts to isolate the absorptions due to the excess proton in dilute acids (e.g., by subtraction of the counterion spectral features, etc.[86, 92]) have yielded similarly diffuse absorptions, which provide little structural information about the local molecular environment of the embedded proton. Indeed, the diffuse background absorption attributed to the positive charge is often referred to as the Zundel continuum[93, 94, 95] in honor of Georg Zundel, who introduced a polarizable $\text{H}_2\text{O}\cdots\text{H}^+\cdots\text{H}_2\text{O}$ model (hereafter called the H_5O_4^+ Zundel ion), in which a proton is trapped between two water molecules, to conceptually understand the origin of the broadening[88]. The nature of the aqueous proton defect has more recently been treated in several theoretical studies[83, 92, 96, 97, 98, 99, 100, 101] which support a variation of Zundel’s model in the context of the importance of a transient special pair between a hydronium ion and one of the three water molecules in its first hydration shell, the $\text{H}_3\text{O}^+(\text{H}_2\text{O})$ Eigen motif[102, 103]. The special pair formed in this distorted Eigen model is evidenced by their shorter OO distances (≤ 2.4 Å) compared to typical values (2.8 Å) found in neutral water[92, 96].

Because of the inherent spectral complexity of bulk water, gas-phase clusters with precisely determined compositions, $\text{H}^+(\text{H}_2\text{O})_n$, provide attractive model systems that aid in the isolation of the vibrational spectral signatures associated with the excess proton surrounded by a well-defined number of water molecules. The advantages of the clusters, especially

when they can be frozen into well-defined geometries, are that they yield highly structured vibrational spectra that allow one to follow the evolution of the OH stretches associated with the excess charge as water molecules are sequentially added to the assembly. From the theoretical perspective, the entire cluster can then be treated in an electronic structure calculation as a supermolecule, where vibrational spectra of the $3N - 6$ normal modes (where N is the number of atoms) can be obtained for candidate minimum energy structures. We then analyze these trends in the context of the cluster structures as well as the deformations of the electron distributions on the nearby water molecules to understand the factors that drive the large, size-dependent frequency shifts of these spectroscopic signatures. Although the properties of isolated low-temperature clusters are much simpler than that of the bulk liquid, their spectroscopic behavior is nonetheless complex, reflecting the cooperative response of an extended H-bonded network. Our goal here is to isolate the key mechanics that underlie the spectroscopic signatures of the size and temperature controlled clusters featuring the embedded hydronium ion to gain insight and motivate reduced dimensionality models that may be helpful for the larger community studying the nature of the excess proton in water.

4.2 THE ELEMENTARY AQUEOUS CATIONS

We now describe the structural features of the hydronium (H_3O^+) and Zundel H_5O_2^+ ions, as they represent limiting forms of proton accommodation where the excess charge can be qualitatively regarded as either delocalized over the three hydrogen atoms in hydronium or primarily localized on one of them in the Zundel ion. The rotationally resolved vibrational spectrum of the isolated H_3O^+ ion was obtained by Saykally and co-workers in the 1980s[104, 105, 106]. The structure was unambiguously determined to have C_{3v} symmetry with an OH bond length of 0.979 Å and a band origin near 3520 cm^{-1} for the (IR active) doubly degenerate asymmetric OH stretch[104, 107, 108]. The broadband vibrational spectrum of the $n = 4$, H_9O_4^+ ion was first reported by Schwarz in 1977[109] and later refined using the messenger-tagging technique by Okumura and co-workers[110, 111, 112]. The spectra were interpreted in the context of the $\text{H}_3\text{O}^+(\text{H}_2\text{O})_3$ Eigen motif, where the hydronium ion

is sequestered within its first solvation shell. The intense, broad band centered near 2650 cm^{-1} is, therefore, traditionally assigned to the asymmetric OH stretches of the embedded hydronium ion[113]. Note that, although the hydronium ion in the Eigen structure retains C_3 symmetry, its asymmetric OH stretching frequency is dramatically reduced by nearly 900 cm^{-1} upon formation of the first hydration shell. The asymmetric OH stretching fundamentals of the embedded H_3O^+ ions systematically red shift with increasing proton affinity of the ligand (between 370 kJ/mol for Ar and 700 kJ/mol for H_2O)[114].

The situation involving the H_5O_2^+ Zundel ion is more complex. It is clear that it features a proton that is equidistant between two oxygen atoms whose pyramidal OH_2 groups are oriented at roughly 90 degrees relative to one another[115, 116, 117, 118, 119] as evidenced by the rotationally resolved spectra of the asymmetric OH stretching vibrations of the flanking water molecules reported by the Lee group in 1989[111]. The lower energy region of this spectrum, where the bands associated with the bridging proton are found, was first identified in several reports about 10 years ago using either Ar-messenger tagging or infrared multiphoton dissociation (IRMPD)[113, 120, 121, 122, 123, 124, 125, 126]. Although both the IRMPD spectra of the warm ions and the Ar-tagged spectra were somewhat compromised, the Ne-tagged spectrum reported by Hammer et al.[124] finally established the basic pattern in 2005. The pattern of the low-energy bands has been accurately reproduced by full 15-dimensional vibrational calculations [127] using ab initio potential energy and dipole moment surfaces[128] where the transitions near 1000 cm^{-1} can be traced to a Fermi resonance between the parallel displacement of the shared proton and a combination band arising from the OO stretch together with two quanta of a wagging mode involving the flanking water molecules[129]. We now turn our attention to the vibrational structure of the $n = 1$ hydronium ion.

4.2.1 The Hydronium Ion and Its OH Stretching Vibrations

The hydronium ion’s vibrational spectrum was first measured by Saykally with the doubly-degenerate asymmetric OH stretching frequency at $\omega_{a_1} = \omega_{a_2} = 3520 \text{ cm}^{-1}$ [104]. Figure 4.1 shows the two asymmetric and one symmetric OH stretching modes obtained from a har-

monic frequency calculation. The two asymmetric stretching modes are labeled \mathbf{a}_1 and \mathbf{a}_2

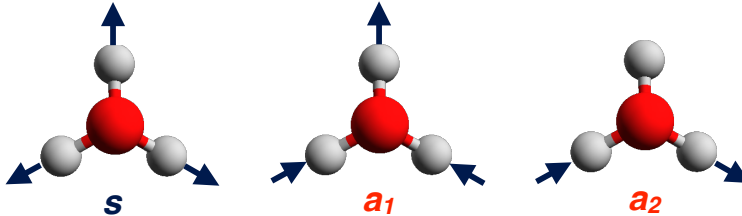


Figure 4.1: The normal modes of an isolated hydronium ion computed at the B3LYP/6-31+G(d) level of theory.

with the frequencies 3606 cm^{-1} , while the symmetric stretching mode is labeled \mathbf{s} with a frequency of 3510 cm^{-1} . Drawing from Section 1.1 and Equation 1.42, the simplest anharmonic potential in this case only includes the cubic couplings between the three normal modes and can be written as

$$H_{3\text{-mode}} = \frac{1}{2} \sum_{i=a_1, a_2, s} \omega_i (p_i^2 + q_i^2) + \frac{1}{6} \sum_{i, j, k=a_1, a_2, s} \phi_{ijk} q_i q_j q_k. \quad (4.1)$$

This shall be referred to as the "3-mode model" in the remaining text. There are 7 relevant cubic coupling constants which contribute to the anharmonicity constants χ_{ij} , which ultimately correct the harmonic frequencies through second-order perturbation theory. These corrected frequencies can be written as

$$\nu_{a_1} = \omega_{a_1} + 2\chi_{a_1 a_1} + \frac{1}{2} (\chi_{a_1 a_2} + \chi_{a_1 s}) \quad (4.2)$$

$$\nu_{a_2} = \omega_{a_2} + 2\chi_{a_2 a_2} + \frac{1}{2} (\chi_{a_2 a_1} + \chi_{a_2 s}) \quad (4.3)$$

$$\nu_s = \omega_s + 2\chi_{ss} + \frac{1}{2} (\chi_{s a_1} + \chi_{s a_2}). \quad (4.4)$$

with the relevant cubic coupling constants listed in Table 4.1. Using Equation 1.54 for the anharmonicity constants χ_{ii} and χ_{ij} gives the 3-mode model frequencies listed in Table 4.2. It must be noted that the Hamiltonian in Equation 4.1 only accounts for the OH stretching modes, neglecting the three bending modes. Accounting for the bending modes and including the quartic couplings gives the full VPT2 Hamiltonian in the space of all normal modes of the hydronium ion, with the resulting anharmonicity constants for the stretching modes shown

modes	$\phi_{ijk}(\text{cm}^{-1})$
$a_1a_1a_1$	285
$a_2a_2a_2$	-1028
sss	-1374
sa_1a_1	-1437
sa_2a_2	-1437
$a_1a_2a_2$	-279
$a_2a_1a_1$	1028

Table 4.1: Cubic coupling constants involving the three OH stretching vibrations of the hydronium ion (cm^{-1}).

	3-mode model (cm^{-1})	VPT2 (cm^{-1})
$\chi_{a_1a_1}$	-46	-49
$\chi_{a_2a_2}$	-47	-49
χ_{ss}	-27	-28
χ_{a_1s}	-111	-114
χ_{a_2s}	-111	-114
$\chi_{a_1a_2}$	- 56	-62

Table 4.2: The anharmonicity constants χ_{ij} contributing to the 3-mode model frequencies and VPT2 frequencies.

in Table 4.2. As shown in Table 4.3, the 3-mode model reproduces the full VPT2 frequencies within $\pm 10 \text{ cm}^{-1}$, showing that the couplings involving the three bending modes do not contribute significantly to the anharmonicity in the gas-phase hydronium ion. Furthermore, this shows that the quartic couplings also contribute very little to the anharmonicity. For

mode	harmonic (cm ⁻¹)	3-mode model (cm ⁻¹)	VPT2 (cm ⁻¹)
a_1	3606	3430	3417
a_2	3606	3431	3422
s	3510	3344	3348

Table 4.3: Harmonic, 3-mode model, and VPT2 vibrational frequencies for the asymmetric OH stretching modes a_1 and a_2 , and the symmetric OH stretching mode s of the bare gas-phase hydronium ion.

capturing only the important interactions between the stretching modes, the 3-mode model is valuable in determining the effects of hydration on the hydronium ion’s OH bonds and shall prove instructive in the remaining text.

4.3 HYDRATION-INDUCED SHIFTS IN THE HYDRONIUM ION’S OH STRETCHING FREQUENCIES

An interesting aspect of the initial spectroscopic survey is that both the $n = 10$ and 21 clusters feature a tri-coordinated, Eigen motif as the charge carrier, but the associated OH stretching vibrations of the embedded hydronium ion are much lower for the $n = 21$ cluster. This raises the important issue that it is not only the local H-bonding environment that governs the vibrational signature but that, somehow, the more distant water molecules dramatically affect the spectroscopic behavior of the charge defect. For this purpose, we first examine the calculated [B3LYP/6-31+G(d)] OH stretch frequencies of H_3O^+ , H_9O_4^+ , and an arrangement of $\text{H}_21\text{O}_{10}^+$ that was chosen to sample the environment of the first and second hydration shells around the hydronium ion as they appear in the minimum energy $\text{H}^+(\text{H}_2\text{O})_{21}$ dodecahedral structure. In the following discussion, we will refer to the optimized $n = 4$ Eigen and $n = 21$ cations as **n4** and **21**, respectively, while frozen structures cut-out from **n21** will

be denoted **n4c** and **n10c**. We now explore the effects of hydration on the OH stretching

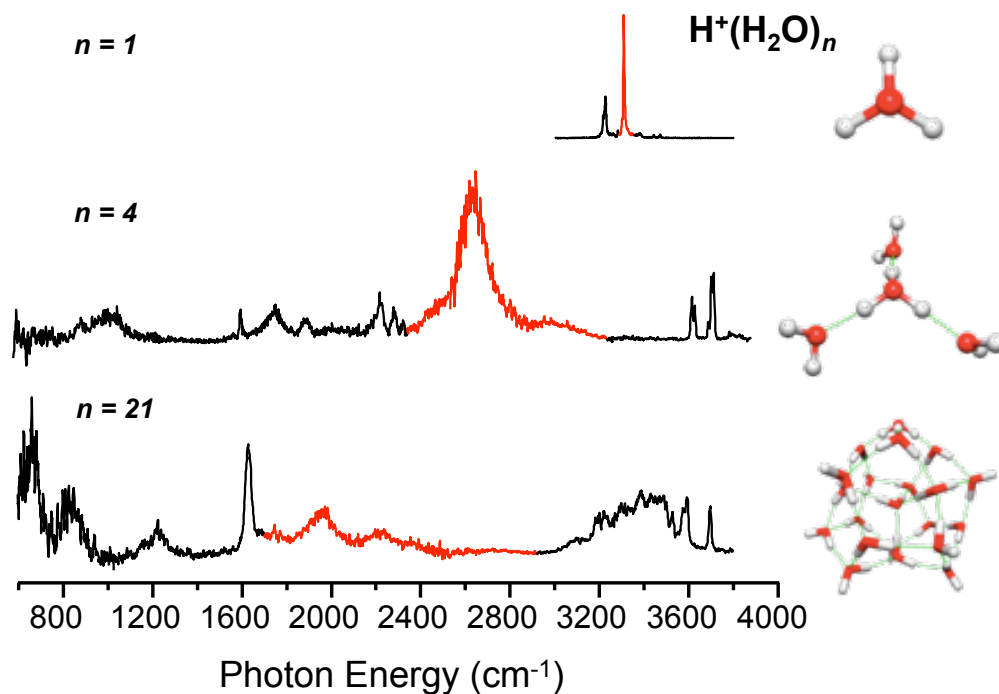


Figure 4.2: The vibrational spectra of the **n1**, **n4**, and **n21** clusters

vibrations of the hydronium ion as shown in Figure 4.2. We first examine the potential energy profile of a hydronium OH bond as it stretches under different hydration conditions. Figure 4.3 shows the geometries considered in the potential energy scan along with their respective labels (with the central hydronium ion colored green for clarity), and Figure 4.4 shows the resulting potential energy curves. Here, the bare hydronium ion (**n1**) is shown in red, the gas-phase Eigen ion (**n4**) in cyan, and the $n = 21$ magic number cluster (**n21**) in black. In order to investigate the effects of geometric distortions resulting from hydration, the OH bond was also scanned for the $n = 4$ (**n4c**) and $n = 10$ (**n10c**) structures shown in Figure 4.3, which are frozen geometries extracted from **n21**. To obtain the $n = 21$ geometry at a reasonably cost-effective level of theory, the second-order Möller-Plesset perturbation theory (MP2) geometry was reoptimized with B3LYP/6-31+G(d), and thus the **n4c** and **n10c** retain the same geometric configuration as in the B3LYP/6-31+G(d) $n = 21$ cluster. We first consider the potential energy curves of the hydronium ion’s OH bond in the relaxed

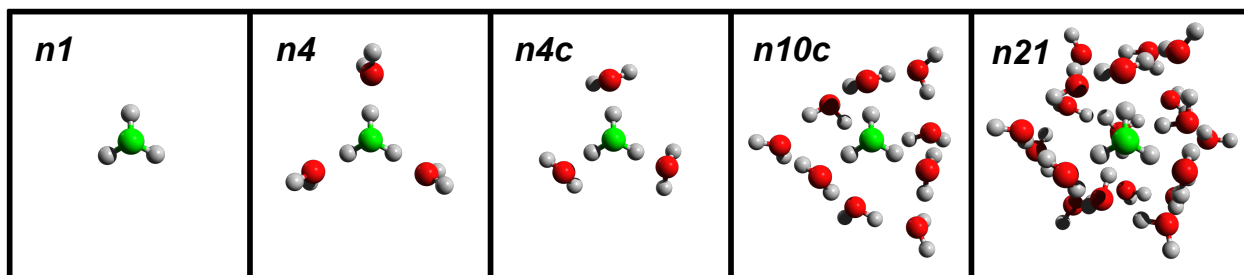


Figure 4.3: Gas-phase geometries used in the potential energy scan of the hydronium ion's OH bond. The structures were fully optimized at the B3LYP/6-31+G(d) level of theory for **n1**, **n4**, and **n21**. For **n4c** and **n10c**, the geometries were extracted from the fully relaxed **n21** geometry followed by optimization of the hydronium ion's OH bonds while freezing all other degrees of freedom.

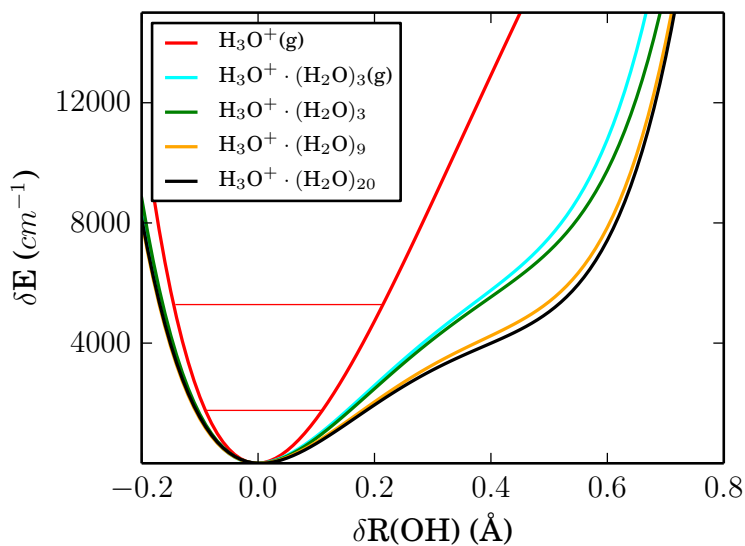


Figure 4.4: The B3LYP/6-31+G(d) potential energy curve of the OH bond of H_3O^+ under the various hydration environments stated in the text.

n1, **n4**, **n21** clusters. The hydronium ion with its "first hydration shell" forms the familiar Eigen ion with C_3 symmetry. Comparing the potential energy curves of **n1** and **n4**, it is

clear that the first hydration shell introduces significant anharmonicity into the hydronium ion’s OH bond and a slight shoulder develops around $R = 0.4 \text{ \AA}$. Upon further hydration to form **n21**, the hydronium ion’s OH bond acquires additional anharmonicity comparable in magnitude to the anharmonicity acquired from the first hydration shell in **n4**. In contrast, the geometric distortions involved in building the **n21** cluster have little influence on the OH bond as evident in the similarities between the **n4c** and **n4** curves, as well as the **n10c** and **n21** curves in Figure 4.4. Therefore, the effects of the electronic interactions between the hydronium ion and its hydration environment plays the dominant role in modifying the OH bonds. Last but not least, the similarities between the **n10c** and **n21** curves indicate that the influence of water molecules beyond the ”second solvation shell” are negligible and therefore the analysis of the intermolecular interactions only considers hydration up to **n10c**.

The intermolecular interactions between the hydronium ion and its hydration shell were analyzed by decomposing the interaction energy using the Symmetry-Adapted Perturbation Theory (SAPT) formalism [77, 78]. SAPT computes the interaction energy decomposed into electrostatic, exchange, polarization, dispersion, and charge-transfer contributions. First, the interaction between the hydronium ion and its first hydration shell, composed of three water molecules, was decomposed within the SAPT2 approximation [79, 80]. Then, the interaction between the hydronium ion and its first two hydration shells were decomposed, with the hydration shell consisting of the water molecules in **n10c**. The interaction energy components are listed in Table 4.4 for **n4** and **n10c**. The interaction between the hydronium ion and its first hydration shell is dominated by electrostatics and polarization. The electrostatic contribution can be interpreted as the Coulomb interaction between the frozen electron densities of the hydronium ion and the first hydration shell in **n4** and the first two hydration shells in **n10c**. This interaction is stabilizing due to the interactions between the partial positive charges on the hydronium ion’s H atoms and the partial negative charges of the hydration shell’s O atoms. The polarization energy is the next major contribution to the total interaction between the hydronium ion and its hydration environment and are listed in Table 4.4. This stabilizing interaction can be interpreted as arising from the induced change in the electron density of the hydronium ion due to the frozen electron density of the hydration shell, and vice versa. The charge transfer interaction contributes only a minor

SAPT2 contribution	n4 (kcal/mol)	n10c kcal/mol
electrostatics	-80.84	-117.50
exchange	71.14	74.34
dispersion	-8.84	-9.56
polarization	-40.10	-47.01
charge-transfer	-8.10	-8.36

Table 4.4: The SAPT2 decomposition of the interactions between the hydronium ion and its first hydration shell (**n4**) and its first two hydration shells (**n10c**) in units of kcal/mol.

amount to the stabilization energy. The SAPT interaction energy components along the OH bond show an increase in stabilizing interactions at longer OH bond lengths, as shown in Figure 4.5. Indeed, the polarization of the OH bond increases dramatically with OH bond stretching as shown in purple. The charge-transfer interaction also increases in stabilizing strength with increasing OH bond length. This can be attributed to an increase in the overlap of the hydronium ion and hydration shell’s wavefunctions as the proton displaces closer to the hydrogen-bonded water molecule.

Due to the importance of the polarization term, it is instructive to examine the change in the electron densities of **n4** and **n10c** due to the intermolecular interactions. Figure 4.6 shows the electron density change for **n4** and **n10c** arising from the polarization-dominated intermolecular interactions between the hydronium ion and its hydration shells. The **n4** density change shows an increase of electron density in the hydrogen bond region of the first hydration shell, both accompanied by corresponding decreases in the electron density around regions separated from the hydrogen bonds by one atom. This suggests that the formation of the first hydration shell around the hydronium ion is indeed dominated by polarization interactions, resulting in the electron density changes shown in Figure 4.6 labeled **n4** and **n10c**. The figure also shows that the formation of the second hydration shell reinforces this polarization interaction with more electron density due to the added water molecules.

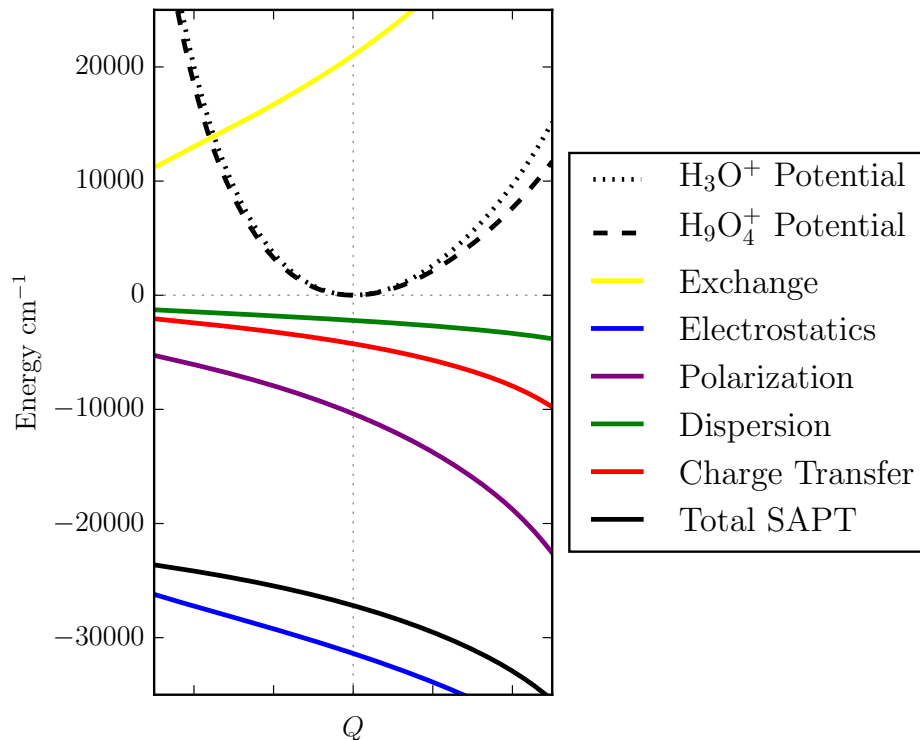


Figure 4.5: The interaction energy contributions as a function of the proton displacement.

Finally, **n10c-2** in Figure 4.6 shows the density changes of the second hydration shell due to the intermolecular interactions between the hydronium ion and its first hydration shell, showing that the hydronium ion does not polarize significantly due to the second hydration shell. In fact, the density changes suggest that the majority of the stabilization energy upon forming the second hydration shell is due to the polarization of the second hydration shell. The strong polarization interaction of the system results in the hydronium ion's OH bonds stretching with successive hydration shells from 0.980 Å to 1.014 Å in **n4** and to 1.030 Å in **n10c**. This bond stretching coupled with the fact that the largest change in the interaction energies when going from **n4** to **n10c** is the stabilizing electrostatic interaction suggests that the increase in the electric field strength of the hydration shell upon the addition of more water molecules is responsible for the dramatic red shift going from the hydronium ion, to the Eigen ion, and to the **n21** cluster. It must be noted that, although several low-lying isomers

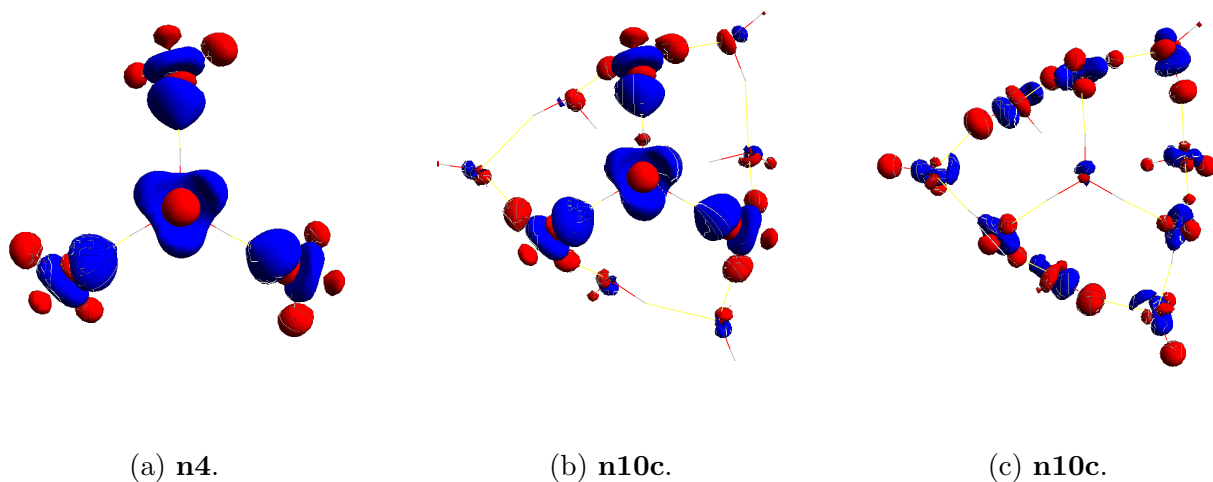


Figure 4.6: Interaction-induced electron density changes calculated at the B3LYP/6-31+G(d) level of theory, with the positive change in electron density colored blue and negative change in electron density colored red.

of the $n = 21$ cluster may be present experimentally, such isomers [130] would have identical arrangements in the first and second solvation shells of the hydronium cation (i.e., similar skeletons of the **n4** and **n10c** isomers), and as such, we would expect very minor variations in the analysis of the important long-range intermolecular interactions. Moreover, although more sophisticated and quantitative models are clearly warranted, most of the underlying physics accounting for the change in the hydronium's OH stretching frequency as a function of the local environment can indeed be described using the simple one-dimensional potentials displayed in Figure 4.4.

Now we examine the three OH stretching vibrational modes of the hydronium ion as a function of hydration using the **n4** and **n10c** clusters. The potential energy scan along the hydronium ion's OH bond showed that the potentials of **n10c** and **n21** were very similar, thus the **n10c** cluster can be used to model the **n21** cluster at a lower computational cost due to the decrease in the number of degrees of freedom. The hydronium ion's OH stretching

frequencies were computed at three different levels of theory (harmonic, 3-mode, and full VPT2) for the **n1**, **n4**, and **n10c** clusters, and the results are listed in Table 4.5. In the

method	mode	n1 (cm ⁻¹)	n4 (cm ⁻¹)	n10c (cm ⁻¹)
harmonic	<i>s</i>	3510	2990	2822
	<i>a</i> ₁	3606	2869	2604
	<i>a</i> ₂	3606	2868	2590
3-mode	<i>s</i>	3344	2718	2664
	<i>a</i> ₁	3430	2547	2242
	<i>a</i> ₂	3431	2551	2229
VPT2	<i>s</i>	3348	2664	2617
	<i>a</i> ₁	3417	2599	2100
	<i>a</i> ₂	3422	2620	2073

Table 4.5: Vibrational frequencies of the hydronium ion’s three OH stretching modes in the bare ion (**n1**), with its first hydration shell (**n4**), and with its first and second hydration shells (**n10c**). The symmetric stretch mode is *s* while the doubly degenerate asymmetric stretch modes are *a*₁ and *a*₂.

harmonic regime, the *a*₁ mode’s frequency shifts from 3606 cm⁻¹ in the hydronium ion to 2869 cm⁻¹ upon addition of the first hydration shell, and to 2604 cm⁻¹ upon further hydration with the second hydration shell. The anharmonicity induced by the first hydration shell results in a broadening of the approximate harmonic potential, bringing the energy levels closer resulting in the large 737 cm⁻¹ red shift. The harmonic approximation does not include couplings between the normal modes, therefore the anharmonicity in the **n4** cluster originates mostly from the polarization of the OH bonds by the hydration shell. This is in contrast to the addition of the second hydration shell, which shows only modest changes in the harmonic frequencies, suggesting that the additional anharmonicity induced by the second hydration shell is due mostly to the couplings between the normal modes. In fact the anharmonicity constants show a clear dependence on the hydration environment, as shown in Table 4.6. Here, the antisymmetric stretch modes show large changes in their

diagonal anharmonic constants when going from **n1** to **n4** while the symmetric stretch mode shows very little change, supporting the idea that the first hydration shell introduces anharmonicity through the intermolecular interactions between the hydronium ion and the surrounding water molecules, while the second hydration shell induces anharmonicity from stronger couplings between the modes.

χ_{ij}	n1 (cm ⁻¹)	n4 (cm ⁻¹)	n10c (cm ⁻¹)
<i>ss</i>	-28	-40	-41
<i>a₁a₁</i>	-49	-118	-152
<i>a₂a₂</i>	-49	-118	-164
<i>sa₁</i>	-114	-246	-327
<i>sa₂</i>	-114	-239	-260
<i>a₁a₂</i>	-62	-109	-80

Table 4.6: The full VPT2 anharmonicity constants involving the hydronium ion’s three OH stretching modes in the bare ion (**n1**), with its first hydration shell (**n4**), and with its first and second hydration shells (**n10c**).

The anharmonicity constants χ_{ij} are themselves functions of the force constants ϕ_{ijk} and ϕ_{iijk} . The dominant terms are the cubic force constants involving the three OH stretch modes of the hydronium ion, and the important ones are listed in Table 4.7. The force constants involving the symmetric stretch mode *s* change significantly when going from **n1** to **n4**, while the change induced by the second hydration shell is three times smaller. In contrast the force constants involving the asymmetric stretch modes show the greater change when going from **n4** to **n10c**, especially in the terms coupling the two degenerate modes. This is due to the loss of the C_3 symmetry of the Eigen ion upon the addition of the second hydration shell breaking the degeneracy of the two asymmetric stretch modes, resulting in larger off-diagonal anharmonic constants, and larger force constants coupling the two. It must be noted that the force constants listed in Table 4.7 are the only force constants in the 3-mode model vibrational Hamiltonian, while the full VPT2 Hamiltonian includes up to the semi-quartic force constants, as shown in Section 1.2.2. For the addition of the first hydration shell, the

3-mode model and full VPT2 frequencies agree within 100 cm^{-1} which indicates that the anharmonicity in **n4** is not due to the strong couplings of the three hydronium OH stretching modes to the other modes of the cluster. The addition of the second hydration shell shows a larger difference between the 3-mode model and full VPT2 frequencies compared to the first hydration shell. This discrepancy can be attributed to the inclusion of the coupling of the three OH stretch modes to the other modes of the clusters, and to the breaking of the C_3 symmetry which induces a change in the couplings strengths.

ϕ_{ijk}	n1 (cm^{-1})	n4 (cm^{-1})	n10c (cm^{-1})
sss	-1374	-1428	-1424
$a_1a_1a_1$	285	922	-286
$a_2a_2a_2$	-1028	928	-1500
$a_s a_1 a_1$	-1437	-1656	-1744
$a_s a_2 a_2$	-1437	-1648	-1636
$a_1 a_2 a_2$	1028	-934	1271
$a_2 a_1 a_1$	-279	-912	357

Table 4.7: The cubic force constants of the symmetric and doubly-degenerate asymmetric mode of hydronium in the bare ion (**1**), with its first hydration shell (**n4**), and with its first and second hydration shells (**n10c**).

4.3.1 The field effect in the proton-transfer mechanism in water

Perhaps the most interesting aspect of connecting cluster behavior to that of the bulk is the extrapolation of the potential curves in Figure 7 to the bulk limit. It is evident that the shelf-like potential calculated for the Eigen cation evolves toward a second minimum upon addition of the next solvation shell. Indeed, were all the atoms allowed to relax as the proton is displaced, this curve would converge to a double-well potential in the bulk limit, with the two minima separated by the proton-transfer barrier. We now turn our attention to the implications of the field effect described above in the proton-transfer mechanism proposed

by Grotthuss [131].

Proton-transfer in aqueous solutions occurs through hopping of the proton from one molecule to another, or rather the exchange of protons between adjacent of water molecules [131]. This process occurs through thermal fluctuations in the hydration environment of the proton passing through transient metastable states, the two extremes of which are the Eigen and Zundel ions [132]. The fluctuation of the proton's hydration environment between these two forms is the reason for the extremely diffuse OH stretching signature of the hydrated proton. Thus the experimental probing of the proton transfer mechanism through vibrational spectroscopy is hampered by the unresolved proton band. In this work, size-selected frozen clusters were constructed so as to capture snapshots along the proton-transfer coordinate. Whereas the previous section focused on the Eigen form of the hydrated proton (as it is the stable structure in the three-dimensional cage configurations), this section will focus on the Zundel form where the proton is equidistant from the oxygen atoms of two adjacent water molecules. If one assumes that the proton-transfer mechanism goes from the Eigen ion to the Zundel ion, followed by another Eigen ion displaced from the original Eigen ion, the Zundel structure represents the halfway point between the initial and final states. It was found that this configuration has an anomalously large polarizability due to the bridging proton's mobility under applied electric fields and contributes to the diffuseness of its spectral signature.

In the previous section, the influence of the hydration environment's electric field on the hydronium ion's OH bonds was shown to result in the observed shelf in the bond potential energy curve of the Eigen ion. This shelf is reinforced when the second hydration shell is added. The second hydration shell of the hydronium ion is an important part of proton transfer as its configuration determines the proton transfer path. In the cryogenically-cooled cluster regime, it is possible to solvate only one of the three water molecules of the first hydration shell with entities possessing increasingly stronger proton affinities. As the proton affinities increase, the hydronium ion's excess proton is pulled towards the solvated water molecule until it is at the midway point, and thus inducing the formation of the Zundel ion. Alternatively, one may asymmetrically solvate the Zundel ion to displace its proton towards forming a hydronium ion with the solvated water molecule. The research group of Prof.

Mark Johnson at Yale university collected these spectral snapshots by first eliminating the crowding of the spectra due to overtones by isotopic substitutions, and then constructing the Eigen cluster solvated on one water molecule by proton acceptors of increasing strength. Figure 4.7 shows a diagram of the Zundel configuration solvated by two proton acceptors on one side and two water molecules on the other side. The figure depicts an Eigen ion under asymmetric solvation by proton acceptors distorting towards the Zundel configuration.

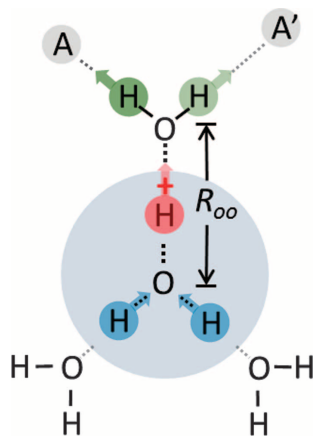


Figure 4.7: Schematic of the Zundel ion under the influence of proton acceptors.

The polarization of the Zundel configuration towards the Eigen configuration is the result of the shift in the proton's position between the two water molecules as stated before. Therefore, the effects of the proton acceptors responsible for the polarization can be modeled by applying an external electric field to the Zundel ion. We first show the potential energy scan of the central proton as it displaces along the axis connecting the two oxygen atoms in Figure 4.8. In Zundel's model for the breadth of the hydrated proton spectrum (13), the potential that governs the parallel vibration of the excess proton is strongly perturbed by the electric field of the solvent surrounding the H_5O_2^+ moiety. This effect arises because of the very large mechanical contribution to the polarizability due to field-induced displacement of the central proton. The calculations for the potential scan were carried out for O-O separations of 2.40, 2.48, and 2.57 Å, with the corresponding fields being 0.00, 51.4, and 103 MV/cm. These O-O distances span the range experienced by the untagged and tagged Eigen complexes, and the fields of 51.4 and 103 MV/cm correspond roughly to those experi-

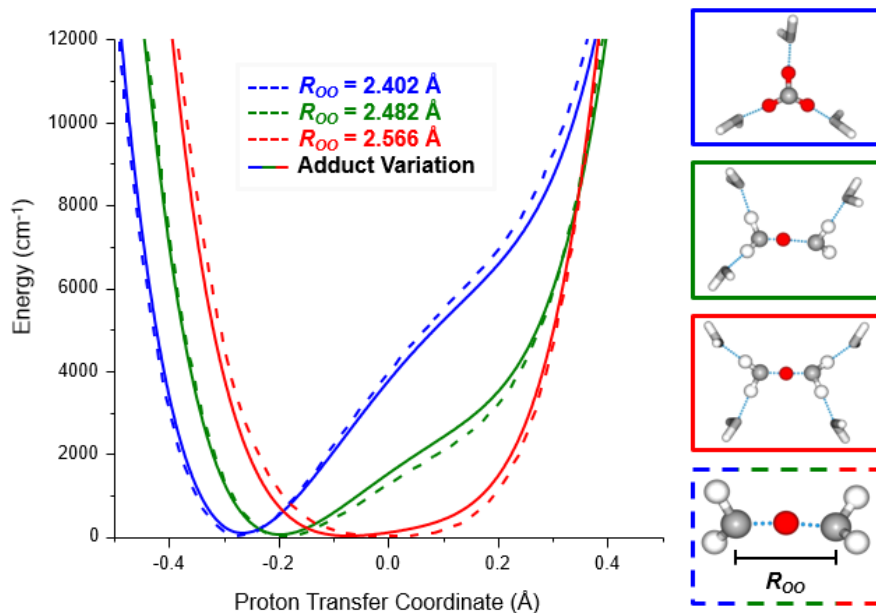


Figure 4.8: Solid lines: scans for the potential energy for displacement of the central proton between the special pair of O atoms for H_9O_4^+ ion (blue), $\text{H}_{11}\text{O}_5^+$ (green), and the Zundel-based isomer of $\text{H}_{13}\text{O}_6^+$ (red) evaluated at the MP2/aug-cc-pVDZ level of theory; dotted lines: potentials for proton displacement in the isolated H_5O_2^+ Zundel ion placed in uniform electric fields with magnitudes simulating those of the hydration shell.

enced by the proton in the Zundel structure when tagged with one or two water molecules, respectively. The close agreement between the two sets of potentials strongly supports the interpretation that the main effect of one or more tags is the modification of the electric field on the shared proton. Figure 4.9 shows the change in the electron density of the Zundel ion under the influence of electric fields of increasing strength. The z -coordinates of the atoms are marked by the vertical dashed lines, while the OO axis is marked by the horizontal dashed line. It is clear that the modified electric field experienced by the central proton upon asymmetric solvation with a proton acceptor results in the polarization of the electron density of the central proton towards the solvated water molecule, creating a displaced po-

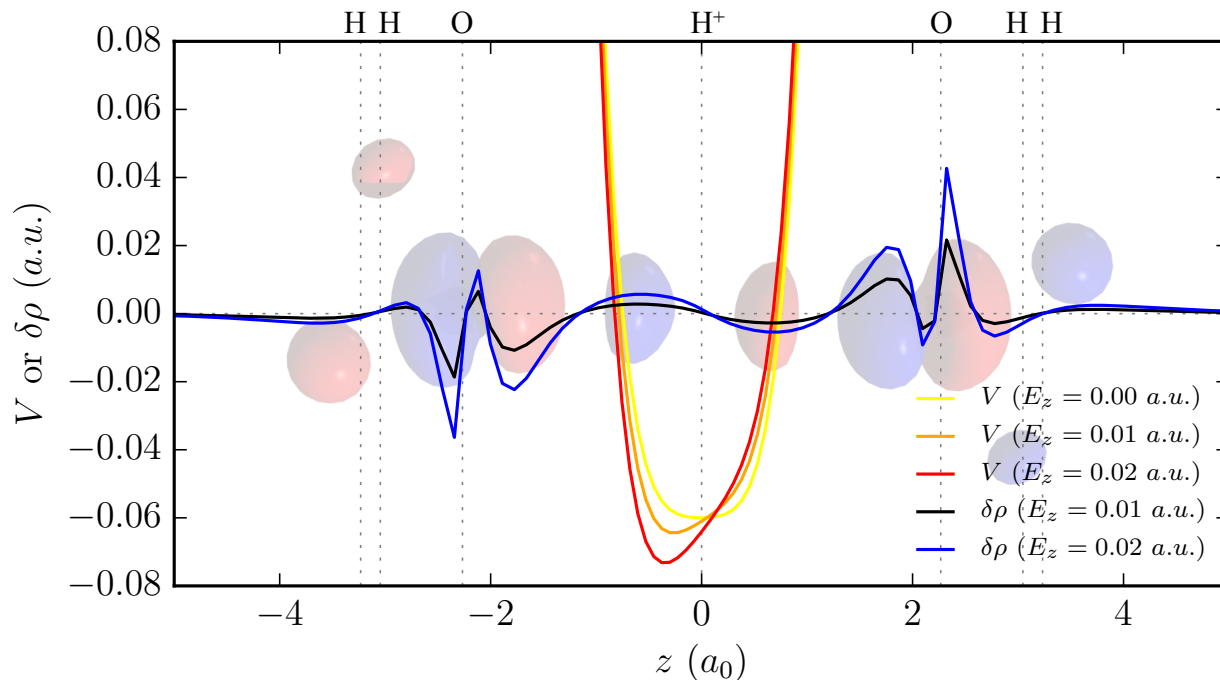


Figure 4.9: A one-dimensional cut through the charge density difference of the Zundel ion under different external electric fields computed at the B3LYP/aug-cc-pVTZ level of theory, overlaid with the central proton’s potential energy curve, as well as the three-dimensional density difference isosurface.

tential energy minimum which gets closer to the Eigen motif with increasing field strength. Therefore, the field effect is involved in the Grotthuss proton-transfer mechanism via the rearrangement of the second hydration shell around the excess proton, with the hydronium ion and the Zundel ion as the two limiting structures.

4.4 EXTRAPOLATING THE CLUSTER MODEL TO BULK WATER

The gas-phase cluster approach to disentangling the vibrational spectrum of protonated water provides deep insight into the underlying physics of proton hydration at very low temperatures. However, the ultimate system to study would be bulk water (at room tem-

perature), hence the validity of extrapolating cluster model properties and mechanisms to bulk water must be discussed. To this end, we consider the $n = 21, 24,$ and 28 clusters, whose vibrational spectra are shown in Figure 4.10. The vibrational features associated with the surface-embedded H_3O^+ that were identified earlier in the $n = 21$ spectrum [133] remain in the same vicinity in the $n = 24$ and 28 clusters but broaden and become less pronounced relative to the increasing contribution from the additional water molecules, both in the region of the diffuse OH stretching vibrations and in the region of the sharper OH bending transitions. By $n = 28$, the entire vibrational spectrum resembles that of bulk dilute acid,

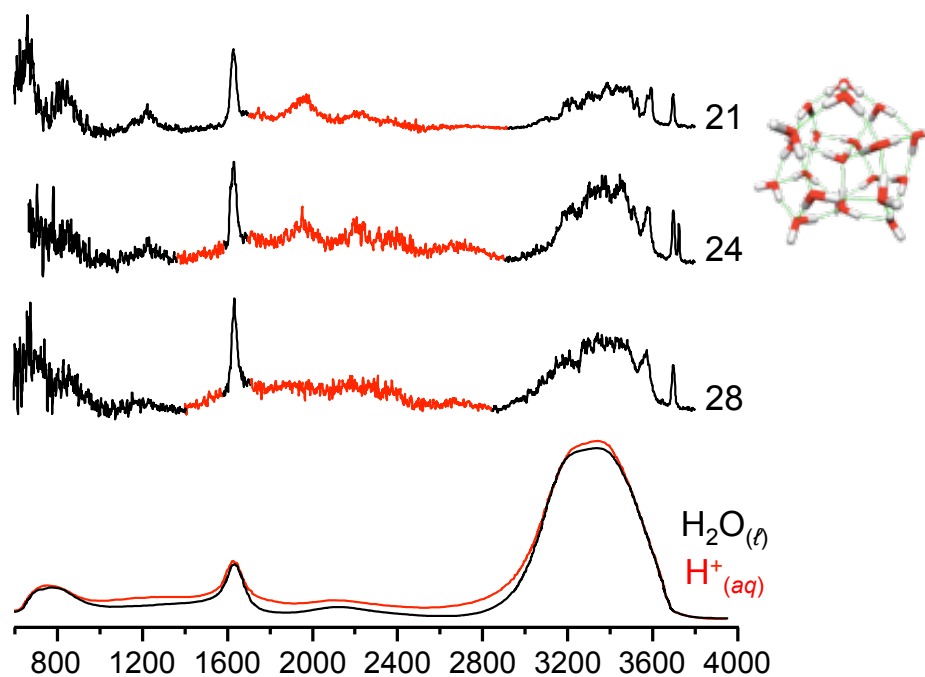


Figure 4.10: The vibrational spectra of $\text{H}^+(\text{H}_2\text{O})_{n=21,24,28}$ clusters compared to the spectra of bulk water and bulk dilute acid.

with the exception of the free OH transition highest in energy at 3700 cm^{-1} , which clearly is not available when the H-bonding becomes saturated with four-coordinated sites in a bulk environment. Recent molecular dynamics simulations by Voth and co-workers [92, 97] explain the observed absorption continuum in the liquid in terms of a dynamically distorted Eigen structure, where Zundel-type motifs exist only as transient proton hopping intermediates. However, it is clear that the hydronium ion remains nearly three-fold symmetric in

both the cryogenically frozen magic $n = 21$ and 28 clusters. The fact that both the position and breadth of the hydronium vibrational signatures (the stretches and the umbrella bending mode) in the $n = 21 - 28$ clusters are close to those in $\text{H}^+(\text{aq})$ suggests that these moderately sized clusters explore many of the local interactions exhibited by the charge defect in liquid water. Interestingly, simulations in both liquid water [134] and ice [135] show that the formation of a four coordinated H_3O^+ by addition of a hydrogen bond donor is unfavorable due to the low charge density around the hydronium oxygen. This is likely why the hydronium resides on the surface of the clathrate-like cages, as opposed to being sequestered in the interior of the cluster [136]. The importance of this fourth water molecule donating an H-bond to the hydronium in the bulk, however, has recently been revisited [100]. Of course, the dynamical behavior exhibited in the bulk will undoubtedly play an important role in the observed spectrum, including nuclear quantum effects [101, 137, 138], where the proton delocalization is almost certainly due to the 300 K temperature. The clusters prepared by the Johnson group are at 10 K, and as a result, they are solid-like and proton delocalization will be much less important. At the low temperatures relevant for the present experiments, the dominant quantum effect is zero-point motion, which is known to couple soft modes to strongly H-bonded stretches [139, 140]. We believe that this is a major factor responsible for the large widths of the features associated with the hydronium OH stretch vibrations in the cold clusters. Important future directions will involve a more quantitative explanation for the spectral breadth as well as determination of the temperature dependence of the spectral patterns.

BIBLIOGRAPHY

- [1] A. J. Stone. *The Theory of Intermolecular Forces*. Oxford University Press, 2 edition, 2013.
- [2] F. Wang and K. D. Jordan. A Drude-model approach to dispersion interactions in dipole-bound anions. *The Journal of Chemical Physics*, 114:10717, 2001.
- [3] F. Wang and K. D. Jordan. Application of a Drude model to the binding of excess electrons to water clusters. *The Journal of Chemical Physics*, 116:6973, 2002.
- [4] Andrew P. Jones, Jason Crain, Vlad P. Sokhan, Troy W. Whitfield, and Glenn J. Martyna. Quantum drude oscillator model of atoms and molecules: Many-body polarization and dispersion interactions for atomistic simulation. *Physical Review B*, 87:144103, 2013.
- [5] R. A. Tkatchenko, A. Ambrosetti, and R. A. DiStasio Jr. Interatomic methods for the dispersion energy derived from the adiabatic connection fluctuation-dissipation theorem. *The Journal of Chemical Physics*, 138:074106, 2013.
- [6] D. C. Langreth and J. C. Perdew. Exchange-correlation energy of a metallic surface: Wave-vector analysis. *Physical Reviews B*, 15:2884, 1977.
- [7] E. M. Myshakin, K. D. Jordan, and M. A. Johnson. Large anharmonic effects in the infrared spectra of the symmetrical $\text{CH}_3\text{NO}_2 \cdot (\text{H}_2\text{O})$ and $\text{CH}_3\text{CO}_2 \cdot (\text{H}_2\text{O})$ complexes. *The Journal of Chemical Physics*, 119:10138, 2003.
- [8] Jeffrey M. Headrick, Eric G. Diken, Richard S. Walters, Nathan I. Hammer, Richard A. Christie, Jun Cui, Evgeniy M. Myshakin, Michael A. Duncan, Mark A. Johnson, and Kenneth D. Jordan. Spectral signatures of hydrated proton vibrations in water clusters. *Science*, 308:1765, 2005.
- [9] Patrick Ayotte, Gary H. Weddle, Christopher G. Bailey, Mark A. Johnson, Fernando Vila, and Kenneth D. Jordan. Infrared spectroscopy of negatively charged water clusters: Evidence for a linear network. *The Journal of Chemical Physics*, 110:6268, 1999.
- [10] Joseph R. Roscioli, Nathan I. Hammera, Mark A. Johnson, Kadir Diri, and Kenneth D. Jordan. Exploring the correlation between network structure and electron

- binding energy in the $(\text{H}_2\text{O})_7(\text{H}_2\text{O})_7$ cluster through isomer-photoslected vibrational predissociation spectroscopy and ab initio calculations: Addressing complexity beyond types I-III. *The Journal of Chemical Physics*, 128:104314, 2008.
- [11] P. Drude. Zur Elektronentheorie der Metalle. *Annalen der Physik*, 306:566–613, 1900.
- [12] E. Harder, A. D. MacKerell, Jr., and B. Roux. Many-body polarization effects and the membrane dipole potential. *Journal of the American Chemical Society*, 131:2760, 2009.
- [13] A. Savelyev and A. D. MacKerell Jr. Allatom polarizable force field for dna based on the classical drude oscillator model. *The Journal of Computational Chemistry*, 35:1219, 2014.
- [14] J. Huang, P. E. M. Lopes, B. Roux, and A. D. MacKerell, Jr. Recent advances in polarizable force fields for macromolecules: microsecond simulations of proteins using the classical drude oscillator model. *The Journal of Physical Chemistry Letters*, 5:3144, 2014.
- [15] C. Schröder and O. Steinhauser. Simulating polarizable molecular ionic liquids with drude oscillators. *The Journal of Chemical Physics*, 133:154511, 2010.
- [16] A. Tkatchenko, R. A. DiStasio, R. Car, and M. Scheffler. Accurate and efficient method for many-body van der waals interactions. *Physical Review Letters*, 108:236402, 2012.
- [17] A. Jones, A. Thompson, J. Crain, M. Muser, and G. Martyna. Norm-conserving diffusion Monte Carlo method and diagrammatic expansion of interacting Drude oscillators: Application to solid xenon. *Physical Reviews B*, 79:144119, 2009.
- [18] H. B. G. Casimir and D. Polder. The influence of retardation on the London-van der Waals forces. *Physical Reviews*, 73:360, 1948.
- [19] T. Takada, M. Dupuis, and H. F. King. Molecular symmetry. III. Second derivatives of electronic energy with respect to nuclear coordinates. *The Journal of Chemical Physics*, 75:332, 1981.
- [20] J. A. Boatz and M. S. Gordon. Decomposition of normal-coordinate vibrational frequencies. *The Journal of Physical Chemistry*, 93:1819, 1989.
- [21] M. J. Frisch, G. W. Trucks, H. B. Schlegel, G. E. Scuseria, M. A. Robb, J. R. Cheeseman, G. Scalmani, V. Barone, B. Mennucci, G. A. Petersson, and et al. *Gaussian 09*. Gaussian, Inc.: Wallingford, CT, 2009.
- [22] V. Barone. Anharmonic vibrational properties by a fully automated second-order perturbative approach. *The Journal of Chemical Physics*, 122:014108, 2005.
- [23] V. Barone, J. Bloino, C. A. Guido, and F. Lipparini. A fully automated implementation of vpt2 infrared intensities. *Chemical Physics Letters*, 496:157, 2010.

- [24] S. Carter, S. J. Culik, and J. M. Bowman. Vibrational self-consistent field method for many-mode systems: A new approach and application to the vibrations of co adsorbed on cu(100). *The Journal of Chemical Physics*, 107:10458, 1997.
- [25] S. Carter J. Koput and N. C. Handy. Ab initio prediction of the vibrational-rotational energy levels of hydrogen peroxide and its isotopomers. *The Journal of Chemical Physics*, 115:8345, 2001.
- [26] P. Cassam-Chenai and J. Lievin. Alternative perturbation method for the molecular vibrationrotation problem. *The International Journal of Quantum Chemistry*, 93:245, 2003.
- [27] J. O. Jung and R. B. Gerber. Vibrational wave functions and spectroscopy of $(\text{H}_2\text{O})_n$, $n = 2, 3, 4, 5$: Vibrational selfconsistent field with correlation corrections. *The Journal of Chemical Physics*, 105:10332, 1996.
- [28] N. Matsunaga, G. M. Chaban, and R. B. Gerber. Degenerate perturbation theory corrections for the vibrational self-consistent field approximation: Method and applications. *The Journal of Chemical Physics*, 117:3541, 2002.
- [29] K. M. Christoffel and J. M. Bowman. Investigations of self-consistent field, scf ci and virtual state configuration interaction vibrational energies for a model three-mode system. *Chemical Physics Letters*, 85:220, 1982.
- [30] V. Barone. Anharmonic vibrational properties by a fully automated second-order perturbative approach. *The Journal of Chemical Physics*, 122:014108, 2005.
- [31] M. W. Schmidt, K. K. Baldrige, J. A. Boatz, S. T. Elbert, M. S. Gordon, J. H. Jensen, S. Koseki, N. Matsunaga, K. A. Nguyen, S. Su, T. L. Windus, M. Dupuis, and J. A. Montgomery. General atomic and molecular electronic structure system. *The Journal of Computational Chemistry*, 14:1347, 1993.
- [32] M. S. Gordon and M. W. Schmidt. *Theory and applications of computational chemistry, the first forty years*. Elsevier, Amsterdam, 2005.
- [33] K. Yagi, K. Hirao, T. Taketsugu, M. W. Schmidt, and M. S. Gordon. *Ab initio* vibrational state calculations with a quartic force field: Applications to H_2CO , C_2O_4 , CH_3OH , CH_3CCH , and C_6H_6 . *The Journal of Chemical Physics*, 121:1383, 2004.
- [34] T. T. Odbadrakh, V. Voora, and K. D. Jordan. Application of electronic structure methods to coupled drude oscillators. *Chemical Physics Letters*, 630:76, 2015.
- [35] A. R. Leach, editor. *Molecular Modeling Principles and Applications*. Addison Wesley Longman, 1996.
- [36] E. Schrödinger. Quantisierung als Eigenwertproblem. *Ann. Phys.*, 80:437, 1926.

- [37] F. Coester and H. Kummel. Short-range correlations in nuclear wave functions. *Nuclear Physics*, 22:477, 1960.
- [38] J. Cizek. On the correlation problem in atomic and molecular systems. Calculation of wavefunction components in Ursell-type expansion using quantum-field theoretical methods. *The Journal of Chemical Physics*, 45:4256, 1966.
- [39] D. J. Thouless. Vibrational states of nuclei in the random phase approximation. *Nuclear Physics*, 22:78, 1961.
- [40] A. D. McLachlan and M. A. Ball. Time-dependent Hartree-Fock theory for molecules. *Review of Modern Physics*, 36:844, 1964.
- [41] H. Eshuis, J. E. Bates, and F. Furche. Electron correlation methods based on the random phase approximation. *Theoretical Chemistry Accounts*, 131:1084, 2012.
- [42] F. London. the general theory of molecular forces. *Transactions of the Faraday Society*, 63:245, 1937.
- [43] A. Szaebo and N. S. Ostlund. The correlation energy in the random phase approximation: Intermolecular forces between closedshell systems. *The Journal of Chemical Physics*, 67:4351, 1977.
- [44] J. Oddeshedde. Polarization propagator calculations. *Advances in Quantum Chemistry*, 11:275, 1978.
- [45] N. Fukada, F. Iqamoto, and K. Sawada. Linearized many-body problem. *Physical Reviews*, 135:A932, 1964.
- [46] A. Hesselmann. Third-order corrections to random-phase approximation correlation energies. *The Journal of Chemical Physics*, 134:204107, 2011.
- [47] J. Toulouse, W. Zhu, A. Savin, G. Jansen, and J. G. Angyan. Closed-shell ring coupled cluster doubles theory with range separation applied on weak intermolecular interactions. *The Journal of Chemical Physics*, 135:084119, 2011.
- [48] G. Scuseria, T. M. Henderson, and D. C. Sorensen. Long-range-corrected hybrids using a range-separated Perdew-Burke-Ernzerhof functional and random phase approximation correlation. *The Journal of Chemical Physics*, 135:084119, 2011.
- [49] R. Moszynski, B. Jeziorski, and K. Szalewicz. MllerPlesset expansion of the dispersion energy in the ring approximation. *The International Journal of Quantum Chemistry*, 45:409, 1993.
- [50] D. J. Rowe. Equations-of-motion method and the extended shell model. *Reviews of Modern Physics*, 40:153, 1968.

- [51] T. T. Odbadrakh and K. D. Jordan. Dispersion dipoles for coupled drude oscillators. *The Journal of Chemical Physics*, 144:034111, 2016.
- [52] C. Moller and M. S. Plesset. Note on an approximation treatment for many-electron systems. *Physical Reviews*, 46:618, 1934.
- [53] R. P. Feynman. Forces in molecules. *Physical Reviews*, 56:340, 1939.
- [54] A. D. Buckingham. *Proprietes optiques et acoustiques des fluides comprimes et actions intermoleculaires*. CNRS, Paris, 1959.
- [55] D. P. Craig and T. Thirunamachandran. Elementary derivation of long-range moments of two coupled centrosymmetric systems. *Chemical Physics Letters*, 80:14, 1981.
- [56] J. O. Hirschfelder and M. A. Eliason. Electrostatic Hellmann-Feynman theorem applied to the long-range interaction of two hydrogen atoms. *The Journal of Chemical Physics*, 47:1164, 1967.
- [57] W. Byers Brown and D. M. Whisnant. Interatomic dispersion dipole. *Molecular Physics*, 25:1385, 1972.
- [58] K. L. C. Hunt. Long-range dipoles, quadrupoles, and hyperpolarizabilities of interaction inert-gas atoms. *Chemical Physics Letters*, 70:336, 1980.
- [59] K. L. C. Hunt and J. E. Bohr. Effects of van der Waals interactions on molecular dipole moments: The role of fieldinduced fluctuation correlations. *The Journal of Chemical Physics*, 83:5198, 1985.
- [60] B. Linder and R. A. Kromhout. van der Waals induced dipoles. *The Journal of Chemical Physics*, 84:2753, 1986.
- [61] L. Galatry and T. Gharbi. The long-range dipole moment of two interacting spherical systems. *Chemical Physics Letters*, 75:427, 1980.
- [62] K. L. C. Hunt. Dispersion dipoles and dispersion forces: Proof of Feynman's "conjecture" and generalization to interacting molecules of arbitrary symmetry. *The Journal of Chemical Physics*, 92:1180, 1990.
- [63] P. Drude. *Lehrbuch der Optik*. S. Hirzel, 1900.
- [64] A. R. Leach. *Molecular Modeling Principles and Applications*. Addison Wesley Longman, 1996.
- [65] D. M. Bishop and J. Pipin. Calculation of the dispersion-dipole coefficients for interactions between H, He, and H₂. *The Journal of Chemical Physics*, 98:4003, 1993.
- [66] H. B. Levine. Role of dispersion in collision-induced absorption. *Physical Review Letters*, 21:1512, 1968.

- [67] M. J. Allen and D. J. Tozer. Helium dimer dispersion forces and correlation potentials in density functional theory. *The Journal of Chemical Physics*, 117:11113, 2002.
- [68] A. D. Dwyer and D. J. Tozer. Dispersion, static correlation, and delocalisation errors in density functional theory: An electrostatic theorem perspective. *The Journal of Chemical Physics*, 135:164110, 2011.
- [69] M. D. Stomsheim, N. Kumar, S. Coriani, E. Sagvolden, A. M. Teale, and T. Helgaker. Dispersion interactions in density-functional theory: An adiabatic-connection analysis. *The Journal of Chemical Physics*, 135:194109, 2011.
- [70] I.-C. Lin, M. D. Coutinho-Neto, C. Felsenheimer, O. A. von Lilienfeld, I. Tavernelli, and U. Rothlisberger. Library of dispersion-corrected atom-centered potentials for generalized gradient approximation functionals: Elements h, c, n, o, he, ne, ar, and kr. *Physical Reviews B*, 75:205131, 2007.
- [71] G. A. DiLabio and O. Otero-de-la Roza. Noncovalent interactions in density-functional theory. *arXiv*, 1405.1771, 2014.
- [72] A. Hesselman. Assessment of nonlocal correction scheme to semilocal density functional theory methods. *Journal of Chemical Theory and Computation*, 9:273, 2012.
- [73] A. Tkatchenko and M. Scheffler. Accurate molecular van der waals interactions from ground-state electron density and free-atom reference data. *Physical Review Letter*, 102:073005, 2009.
- [74] N. Ferri, R. A. DiStasio Jr., A. Ambrosetti, R. Car, and A. Tkatchenko. Electronic properties of molecules and surfaces with a self-consistent interatomic van der waals density functional. *Physical Review Letters*, 114:176802, 2015.
- [75] J. A. Fournier, C. T. Wolke, M. A. Johnson, T. T. Odbadrakh, K. D. Jordan, S. M. Kathmann, and S. S. Xantheas. Snapshots of proton accomodation at a microscopic water surface: Understanding the vibrational spectral signatures of the charge defect in cryogenically cooled $\text{H}^+(\text{H}_2\text{O})_{n=2-28}$. *The Journal of Physical Chemistry A*, 119:9425, 2015.
- [76] C. T. Wolke, J. A. Fournier, L. C. Dzugan, M. R. Fagiani, T. T. Odbadrakh, H. Knorke, K. D. Jordan, A. B. McCoy, K. R. Asmis, and M. A. Johnson. Spectroscopic snapshots of the proton-transfer mechanism in water. *Science*, 354:1131, 2016.
- [77] A. J. Misquitta, R. Podeszwa, B. Jeziorski, and K. Szalewicz. Intermolecular potentials based on symmetry-adapted perturbation theory with dispersion energies from time-dependent density-functional theory. *The Journal of Chemical Physics*, 123:214103, 2205.
- [78] A. J. Stone and A. Misquitta. Charge-transfer in symmetry-adapted perturbation theory. *Chemical Physics Letters*, 473:201, 2009.

- [79] E. G. Hohenstein and C. D. Sherrill. Density fitting of intramonomer correlation effects in symmetry-adapted perturbation theory. *The Journal of Chemical Physics*, 133:014101, 2010.
- [80] T. M. Parker, L. A. Burns, R. M. Parrish, A. G. Ryno, and C. D. Sherrill. Levels of symmetry-adapted perturbation theory (sapt). i. efficiency and performance for interaction energies. *The Journal of Chemical Physics*, 140:094106, 2014.
- [81] J. M. Turney, A. C. Simmonett, R. M. Parrish, E. G. Hohenstein, F. A. Evangelista, J. T. Fermann, B. J. Mintz, L. A. Burns, J. J. Wilke, Abrams., and et al. Psi4: An open-source ab initio electronic structure program. *Computational Molecular Science*, 2:556, 2012.
- [82] D. Marx, M. E. Tuckerman, J. Hutter, and M. Parrinello. The nature of the hydrated excess proton in water. *Nature*, 397:601, 1999.
- [83] T. C. Berkelbach, H. S. Lee, and M. E Tuckerman. Concerted hydrogen-bond dynamics in the transport mechanism of the hydrated proton: A first-principles molecular dynamics study. *Physical Review Letters*, 103:238302, 2009.
- [84] J. Lobaugh and G. A. Voth. The quantum dynamics of an excess proton in water. *The Journal of Chemical Physics*, 104:2056, 1996.
- [85] T. J. F. Day, U. W. Schmitt, and G. A. Voth. The mechanism of hydrated proton transfer in water. *The Journal of the American Chemical Society*, 122:12027, 2000.
- [86] J. Kim, U. W. Schmitt, J. A. Gruetzmacher, G. A. Voth, and N. E. Scherer. The vibrational spectrum of the hydrated proton: comparison of experiment, simulation, and normal mode analysis. *The Journal of Chemical Physics*, 116:737, 2002.
- [87] M. Eigen. Proton transfer, acid-basis catalysis, and enzymatic hydrolysis. *Angewandte Chemie International Edition*, 3:1, 1964.
- [88] Zundel G. Sandorfy C. Schuster, P., editor. *The Hydrogen Bond - Recent Developments in Theory and Experiments. II. Structure and Spectroscopy*. North - Holland, 1976.
- [89] C. J. Fecko, J. D. Eaves, J. J. Loparo, A. Tokmakoff, and P. L. Geissler. Ultrafast hydrogen-bond dynamics in the infrared spectroscopy of water. *Science*, 301:1698, 2003.
- [90] J. J. Loparo, S. T. Roberts, and A Tokmakoff. Multidimensional infrared spectroscopy of water. ii. hydrogen bond switching dynamics. *The Journal of Chemical Physics*, 125:194522, 2006.
- [91] J. J. Loparo, S. T. Roberts, and A Tokmakoff. Multidimensional infrared spectroscopy of water. i. vibrational dynamics in two-dimensional ir line shapes. *The Journal of Chemical Physics*, 125:194521, 2006.

- [92] J. Q. Xu, Y. Zhang, and G. A. Voth. Infrared spectrum of the hydrated proton in water, 2011.
- [93] M. V. Vener and N. B. Librovich. The structure and vibrational spectra of proton hydrates: H_5O_2^+ as a simplest stable ion. *International Reviews in Physical Chemistry*, 28:407, 2009.
- [94] R. Janoschek, E. G. Weidemann, H. Pfeiffer, and G. Zundel. Extremely high polarizability of hydrogen bonds. *The Journal of the American Chemical Society*, 94:2387, 1972.
- [95] G. V. Yukhnevich, E. G. Tarakanova, V. D. Mayorov, and N. B. Librovich. Nature of continuous absorption in ir-spectra of charged complexes with a symmetrical hydrogen-bond. *The Journal of Molecular Structure*, 265:237, 1972.
- [96] O. Markovitch, H. Chen, S. Izenkov, F. Paesani, G. A. Voth, and N. Agmon. Special pair dance and partner selection: Elementary steps in proton transport in liquid water. *The Journal of Physical Chemistry B*, 112:112, 2008.
- [97] C. Knight and G. A. Voth. The curious case of the hydrated proton. *Accounts of Chemical Research*, 45:101, 2012.
- [98] M. Tuckerman, K. Laasonen, M. Sprik, and M. Parrinello. Ab initio molecular dynamics simulation of the solvation and transport of hydronium and hydroxyl ions in water. *The Journal of Chemical Physics*, 103:150, 1995.
- [99] D. Asthagiri, L. R. Pratt, and J. D. Kress. Ab Initio Molecular Dynamics and Quasi-chemical Study of H^+ (Aq). *Proceedings of the National Academy of Sciences U.S.*, 102:6704, 2005.
- [100] Y. L. S. Tse, C. Knight, and G. A. Voth. An analysis of hydrated proton diffusion in ab initio molecular dynamics. *The Journal of Chemical Physics*, 142:014104, 2015.
- [101] A. Hassanali, F. Giberti, J. Cuny, T. D. Kuhne, and M. Parrinello. Proton transfer through the water gossamer. *The Journal of Chemical Physics*, 110:13723, 2013.
- [102] E. Wicke, M. Eigen, and T. Ackermann. über den zustand des protons (hydroniumions) in wässriger lösung. *Z. Phys. Chem.*, 1:340, 194.
- [103] M. Eigen and L. Demaeyer. Self-dissociation and protonic charge transport in water and ice. *Proceedings of the Royal Society of London, Series A*, 247:505, 1958.
- [104] M. H. Begemann, C. S. Gudeman, J. Pfaff, and R. J. Saykally. Detection of the hydronium ion (H_3O^+) by high-resolution infrared spectroscopy. *Physical Review Letters*, 51:554, 1983.

- [105] M. H. Begemann and R. J. Saykally. A Study of the Structure and Dynamics of the Hydronium Ion by High-Resolution Infrared Laser Spectroscopy. I. The ν_3 Band of H_3O^+ . *The Journal of Chemical Physics*, 82:3570, 1985.
- [106] M. Gruebele, M. Polak, and R. J. Saykally. A Study of the Structure and Dynamics of the Hydronium Ion by High-Resolution Infrared Laser Spectroscopy. II. The ν_4 Perpendicular Bending Mode of H_3O^+ . *The Journal of Chemical Physics*, 87:3347, 1987.
- [107] F. Dong and D. J. Nesbitt. Jet Cooled Spectroscopy of H_2DO^+ : Barrier Heights and Isotope-Dependent Tunneling Dynamics from H_3O^+ to D_3O^+ . *The Journal of Chemical Physics*, 125:144311, 2006.
- [108] H. S. P. Muller, F. Dong, D. J. Nesbitt, T. Furuya, and S. Saito. Tunneling Dynamics and Spectroscopic Parameters of Monodeuterated Hydronium, H_2DO^+ , from a Combined Analysis of Infrared and Sub-Millimeter Spectra. *Physical Chemistry Chemical Physics*, 12:8362, 2010.
- [109] H. A. Schwarz. Gas Phase Infrared Spectra of Oxonium Ions from 2 to 5 μ . *The Journal of Chemical Physics*, 67:5525, 1977.
- [110] M. Okumura, L. I. Yeh, J. D. Myers, and Y. T. Lee. Infrared Spectra of the Cluster Ions $\text{H}_7\text{O}_3^+\cdot\text{H}_2$ and $\text{H}_9\text{O}_4^+\cdot\text{H}_2$. *The Journal of Chemical Physics*, 85:2328, 1986.
- [111] L. I. Yeh, M. Okumura, J. D. Myers, J. M. Price, and Y. T. Lee. Vibrational Spectroscopy of the Hydrated Hydronium Cluster Ions $\text{H}_3\text{O}^+(\text{H}_2\text{O})_n$ ($n = 1, 2, 3$). *The Journal of Chemical Physics*, 91:7319, 1989.
- [112] M. Okumura, L. I. Yeh, J. D. Myers, and Y. T. Lee. Infrared-Spectra of the Solvated Hydronium Ion: Vibrational Predissociation Spectroscopy of Mass-Selected $\text{H}_3\text{O}^+(\text{H}_2\text{O})_n(\text{H}_2)$. *The Journal of Physical Chemistry*, 94:3416, 1990.
- [113] J. M. Headrick, E. G. Diken, R. S. Walters, N. I. Hammer, R. A. Christie, J. Cui, E. M. Myshakin, M. A. Duncan, M. A. Johnson, and K. D. Jordan. Spectral signatures of hydrated proton vibrations in water clusters. *Science*, 308:1765, 2005.
- [114] A. B. McCoy, T. L. Guasco, C. M. Leavitt, S. G. Olesen, and M. A. Johnson. Vibrational Manifestations of Strong Non-Condon Effects in the $\text{H}_3\text{O}^+\text{X}_3$ ($\text{X} = \text{Ar}, \text{N}_2, \text{CH}_4, \text{H}_2\text{O}$) Complexes: A Possible Explanation for the Intensity in the Association Band in the Vibrational Spectrum of Water. *Physical Chemistry Chemical Physics*, 14:7205, 2012.
- [115] J. Dai, Z. Bacic, X. Huang, S. Carter, and J. M. Bowman. A theoretical study of vibrational mode coupling in $\text{h}_5 \text{o}_2^+$. *The Journal of Chemical Physics*, 119:6571, 2003.

- [116] X. Huang, H. M. Cho, S. Carter, L. Ojam e, J. M. Bowman, and S. J. Singer. Full Dimensional Quantum Calculations of Vibrational Energies of H_5O_2^+ . *The Journal of Physical Chemistry A*, 107:7142, 2003.
- [117] A. B. McCoy, X. Huang, S. Carter, M. Y. Landeweer, and J. M. Bowman. Full-Dimensional Vibrational Calculations for H_5O_2^+ Using an Ab Initio Potential Energy Surface. *The Journal of Chemical Physics*, 122:061101, 2005.
- [118] O. Vendrell, F. Gatti, and H.-D. Meyer. Strong isotope effects in the infrared spectrum of the zundel cation. *Angewandte Chemie, International Edition*, 48:352, 2009.
- [119] S. S. Xantheas. Dances with hydrogen cations. *Nature*, 457:673, 2009.
- [120] K. R. Asmis, N. L. Pivonka, G. Santambrogio, M. Br mmer, C. Kaposta, D. M. Neumark, and L. W ste. Gas-phase infrared spectrum of the protonated water dimer. *Science*, 299:1375, 2003.
- [121] T. D. Fridgen, T. B. McMahon, L. MacAleese, J. Lemaire, and P. Maitre. Infrared spectrum of the protonated water dimer in the gas phase. *The Journal of Physical Chemistry A*, 108:9008, 2004.
- [122] J. M. Headrick, J. C. Bopp, and M. A. Johnson. *The Journal of Chemical Physics*, 121:11523, 2004.
- [123] E. G. Diken, J. M. Headrick, J. R. Roscioli, J. C. Bopp, M. A. Johnson, and A. B. McCoy. Fundamental Excitations of the Shared Proton in the H_3O_2^- and H_5O_2^+ Complexes. *The Journal of Physical Chemistry A*, 109:1487, 2005.
- [124] N. I. Hammer, E. G. Diken, J. R. Roscioli, M. A. Johnson, E. M. Myshakin, A. B. Jordan, K. D.; McCoy, X. Huang, J. M. Bowman, and S. Carter. The Vibrational Predissociation Spectra of the $\text{H}_5\text{O}_2^+\cdot\text{Rg}_n$ ($\text{Rg} = \text{Ar}, \text{Ne}$) Clusters: Correlation of the Solvent Perturbations in the Free OH and Shared Proton Transitions of the Zundel Ion. *The Journal of Chemical Physics*, 122:244301, 2005.
- [125] L. R. McCunn, J. R. Roscioli, B. M. Elliott, M. A. Johnson, and A. B. McCoy. Why Does Argon Bind to Deuterium? Isotope Effects and Structures of $\text{Ar}\cdot\text{H}_5\text{O}_2^+$ Complexes. *The Journal of Physical Chemistry A*.
- [126] L. R. McCunn, J. R. Roscioli, M. A. Johnson, and A. B. McCoy. An H/D Isotopic Substitution Study of the $\text{H}_5\text{O}_2^+\cdot\text{Ar}$ Vibrational Predissociation Spectra: Exploring the Putative Role of Fermi Resonances in the Bridging Proton Fundamentals. *The Journal of Physical Chemistry B*, 112:321, 2008.
- [127] O. Vendrell and H. D. Meyer. A Proton between Two Waters: Insight from Full-Dimensional Quantum-Dynamics Simulations of the $[\text{H}_2\text{O}-\text{H}-\text{OH}_2]^+$ Cluster. *Physical Chemistry Chemical Physics*, 10:4692, 2008.

- [128] X. Huang, B. J. Braams, and J. M. Bowman. Ab Initio Potential Energy and Dipole Moment Surfaces for H_5O_2^+ . *The Journal of Chemical Physics*, 122:044308, 2005.
- [129]
- [130] S. S. Xantheas. Low-lying energy isomers and global minima of aqueous nanoclusters: Structures and spectroscopic features of the pentagonal dodecahedron $(\text{h}_2\text{o})_{20}$ and $(\text{h}_3\text{o})+(\text{h}_2\text{o})_{20}$. *The Canadian Journal of Chemical Engineering*, 90:843, 2012.
- [131] C. J. D. von Grotthuss. *Ann. Chim.* 1806.
- [132] D. Marx. Proton transfer 200 years after von grotthuss: Insights from ab initio simulations. *ChemPhysChem*, 7:1848, 2006.
- [133] J. A. Fournier, C. J. Johnson, C. T. Wolke, G. H. Weddle, A. B. Wolk, and M. A. Johnson. Vibrational Spectral Signature of the Proton Defect in the Three-Dimensional $\text{H}^+(\text{H}_2\text{O})_{21}$ Cluster. *Science*, 344:1009, 2014.
- [134] Y. J. Wu, H. N. Chen, F. Wang, F. Paesani, and G. A. Voth. An improved multistate empirical valence bond model for aqueous proton solvation and transport. *The Journal of Physical Chemistry B*, 112:467, 2008.
- [135] K. Park, W. Lin, and F. Paesani. Fast and slow proton transfer in ice: The role of the quasi-liquid layer and hydrogen-bond network. *The Journal of Physical Chemistry B*, 118:8081, 2014.
- [136] S. S. Iyengar, M. K. Petersen, T. J. F. Day, C. J. Burnham, V. E. Teige, and G. A. Voth. The properties of ion-water clusters. i. the protonated 21-water cluster. *The Journal of Chemical Physics*, 123:084309, 2005.
- [137] F. Giberti, A. A. Hassanali, M. Ceriotti, and M. Parrinello. The role of quantum effects on structural and electronic fluctuations in neat and charged water. *The Journal of Physical Chemistry B*, 118:13226, 2014.
- [138] M. Ceriotti, J. Cuny, M. Parrinello, and D. E. Manolopoulos. Nuclear quantum effects and hydrogen bond fluctuations in water. *Proceedings of the National Academy of Sciences U.S.A.*, 110:15591, 2013.
- [139] C. J. Johnson, L. C. Dzugan, A. B. Wolk, C. M. Leavitt, J. A. Fournier, A. B. McCoy, and M. A. Johnson. Microhydration of Contact Ion Pairs in $\text{M}_2^+\text{OH}(\text{H}_2\text{O})_{n=15}$ ($\text{M} = \text{Mg}, \text{Ca}$) Clusters: Spectral Manifestations of a Mobile Proton Defect in the First Hydration Shell. *The Journal of Physical Chemistry A*, 118:7590, 2014.
- [140] C. M. Leavitt, A. F. DeBlase, M. van Stipdonk, A. B. McCoy, and M. A. Johnson. Hiding in plain sight: Unmasking the diffuse spectral signatures of the protonated n-terminus in simple peptides. *The Journal of Physical Chemistry Letters*, 4:3450, 2013.